HELIUM NUCLEATION IN LIQUID METALS

A Master's Thesis

Submitted to the Faculty of the

Escola Tècnica d'Enginyeria de Telecomunicació de Barcelona

Universitat Politècnica de Catalunya

by

BORJA PEDREÑO MARTÍNEZ

In partial fulfillment

Of the requirements for the degree of

MASTER IN ENGINEERING PHYSICS

Advisor: Jordi Martí Rabassa & Ferran Mazzanti Castrillejo

Barcelona, November 2020

INDEX

REVISION HISTORY AND APPROVAL RECORD

Revision	**Date**	**Purpose**
0	22/10/2020	Document creation
1	26/10/2020	Document revision
2	03/11/2020	Document revision

Written by:		**Reviewed and approved by:**	
Date	03/11/2020	**Date**	03/11/2020
Name	Borja Pedreño Martínez	**Name**	Jordi Martí Rabassa & Ferran Mazzanti Castrillejo
Position	Project Author	**Position**	Project Supervisors

ACKNOWLEDGEMENTS

Thanks to Jordi Martí and Ferran Mazzanti for the supervision, the advice and the patience while I was doing the work. Thanks also to Agustí Badimon for his help with the Inca cluster to do the simulations.

FIGURES LIST

Chapter I:

Chapter II:

Chapter III:

TABLES LIST

Chapter III

HELIUM NUCLEATION IN LIQUID METALS

Borja Pedreño Martínez

Universitat Politècnica de Catalunya

Departament de Física

ABSTRACT

Obtaining a successful nuclear fusion reaction is a really hard task. One of the factors that we must consider is the high temperatures that the blanket that wraps up the plasma can achieve. Due to this issue, the metals that are used acquire liquid properties, being then a problem when contacting with the helium resulting from the nuclear fusion reaction of tritium. This is due to the fact that helium bubbles are formed at the pressure and temperature conditions that take place in these devices. These bubbles must be studied as that they can compromise the efficiency of the breeding blanket, and thus the efficiency of the reactor. For this purpose, two simulation methods will be used: Monte-Carlo (MC) and Molecular Dynamics (MD). These bubbles were reproduced under controlled conditions at a certain range of pressures, and the results were compared with available experimental data.

I. INTRODUCTION

1.1. The nuclear fusion

The future energy demand is a primary interest issue nowadays. The energetic needing increases everyday and these needs must be fulfilled progressively. One of the fields that has the highest projection while facing the future is the one relying on the nuclear fusion energies. We can obtain large amounts of energy from that source using relatively small quantities of initial matter.

This reaction allows the stars like our Sun to bright and produce thermal energy, as well as other kind of radiation, like UV radiation. In short terms, it allows the stars to work. The main reactions that take place inside of the stars are produced from the hydrogen fusion, from where helium is produced. Besides, heavier elements can be generated as the star runs out of hydrogen, which are then used to enhance the fusion reactions, which results in heavier elements.

The nuclear fusion is highly complicate to manage efficiently in controlled conditions. Extreme pressures and temperatures are needed to achieve conditions that must be sustained during the time needed till the reaction becomes auto-sustainable. For this purpose, we need to set a sufficiently high temperature to allow the reactions to take place and the necessary plasma density to ensure a large probability for the particles to collide. Also, these conditions must be sustained for a certain period of time to harvest the necessary amount of energy to achieve an effective energy gain. This is what we call the Lawson's criteria. This concept establishes the conditions that we need to achieve an effective reaction using as variables the temperature (T), the confinement time (τ), and the plasma density (n).

The ignition temperature is the temperature at which the heating power surpasses the power losses. This temperature changes for some elements. As an example, the ignition temperature for the deuterium-tritium fusion reaction is about T=4.8 keV.

Second, we have also the confinement time. This concept aims for having the plasma over the ignition temperature during a certain time interval. This time must be large enough so as to make the reaction have a net income of energy, superior that the one required to heat the plasma.

Finally, the critical density of ions (n) is the density at which the plasma achieves a collision probability large enough in order to achieve a net income of energy in the reaction.

These last two concepts are expressed using the Lawson criteria, as the product of the density and the ignition time. For the deuterium-tritium reaction, this results in:

$$n\tau \geq 2 \cdot 10^{20}\ s/cm^3 \qquad \textbf{(1)}$$

We have three ways to confine plasma to take place a nuclear fusion reaction: inertial, magnetic and gravitational. For the purpose of this studying, we focus on the magnetic confinement because it is the one that uses the ITER reactor.

The magnetic confinement uses intense magnetic fields to confine the plasma used in the nuclear reactor. No material is able to resist the extreme temperatures that take place at the plasma, so magnetic fields are needed to maintain the plasma in controlled conditions. For that matter we have two different reactors, the tokamak and the stellarator (see Fig 1.1). In the stellarators, all the magnetic field is generated using electric currents applied to helicoidal solenoids at the outside of the plasma. However, if we apply an external force (centripetal force or gravity) in addition to the velocity component that is parallel to the magnetic field, it appears a concept called drift velocity, which deviates the particles inside the ring structure. This critical issue is overcome adding a poloidal component of the magnetic field that compensates this deviation.

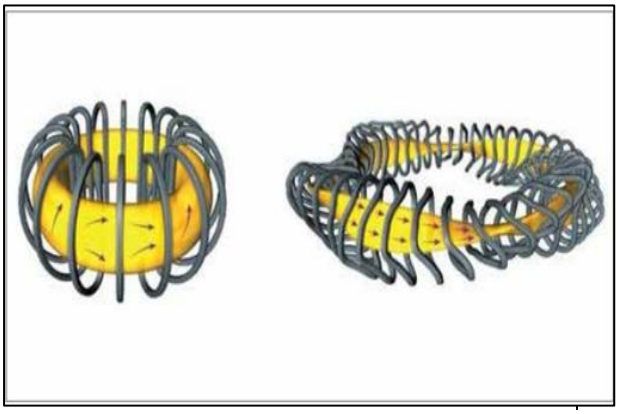

Figure 1.1: Tokamak structure (left) and stellarator structure (right).

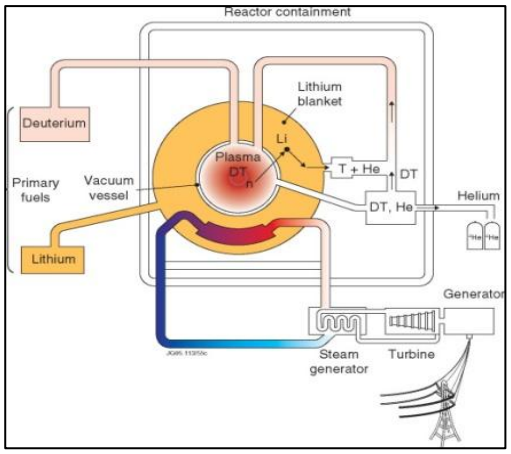

Figure 1.2: Scheme of a fusion power plant.

This is an issue that makes the stellarators highly complex, but it is easily overcome at the tokamaks. In these structures, an electrical current is applied across the plasma, generating a poloidal component that maintains the plasma confined.

To understand the process that we are analyzing, it is necessary to know how a fusion energy generation plant works (see Fig. 1.2).

There are some element combinations through which we can achieve an efficient nuclear fusion reaction. The most used is the one that corresponds to deuterium and tritium in plasma. As said previously, this plasma must be at extremely high temperatures, even of the order of millions of degrees, and at pressures of the order of the GPa.

Obtaining deuterium is a relatively easy task. With the proper enrichment it can be obtained from the terrestrial surface water. Obtaining tritium is way more complicated. Its production in nature is very rare, being the result of the interaction of cosmic rays with the atmosphere. However, this process generates insignificant quantities of tritium.

The human production of tritium is also highly limited when we are talking about storing it. Due to this problem, tritium has to be produced inside the reactor using neutron capture reactions on lithium. The general equation of this reaction is written as follows:

$$^{6}_{3}Li + ^{1}_{0}n \rightarrow ^{4}_{2}He + ^{3}_{1}T + 4{,}7MeV \quad \textbf{(2)}$$

We can see that helium is a by-product of this reaction. We will discuss this issue later, because it is critical in the problem that appears in the blanket of the reactor.

The collect of energy is not very different from the techniques employed in other systems like thermal power plants or fission power plants. The generated power heats water, which is then evaporated and goes towards a turbine where there is an alternator that spins propelled by this steam, producing electric power. Then the steam is cooled and condensed, returning to the circuit

and evacuating the excess of heat to an exterior focus to be reused again.

1.2. The ITER

The ITER (International Thermonuclear Experimental Reactor) started in 1985 and is one of the most ambitious scientific energy projects that we have nowadays in course. It is expected to be the first fusion reactor in the world to produce net energy, being right now the world record of energy production held by the Joint European Torus (JET) fusion reactor. This project will be crucial in the development of the industrial production of fusion-based energy.

The main objective is to produce an income of 500 MW of fusion power from 50 MW of heating power. In other words, it must produce ten times more energy than it is used to start the nuclear reaction.

The reactor uses the tokamak structure and its principal components are:

Field coil system

This system is defined by a central solenoid covered by toroidal field coils (see Fig. 1.3). These coils induce a magnetic field that maintains the plasma partially confined. As we explained before, a drift velocity then appears, which is corrected applying an electrical current across the plasma using a poloidal field system (see Fig. 1.4) that generates a new magnetic component, due to the fact that the plasma is a charged medium.

Vacuum vessel:

Hermetically closed and enveloping the plasma, it is designed to be the first barrier in front of the powerful neutronic field, absorbing the neutron thermal radiation and also the radiation from the plasma, avoiding at the same time the leakage of radioactive particles (see Fig. 1.5).

Divertor:

His function is to catch the particles that are formed from the plasma heating or from the fusion reaction. It is placed at the lower side of the reactor's chamber. It can collect neutral atoms or helium atoms produced at the fusion reaction. Using magnetic fields, these particles are brought to the divertor due to their higher mass compared to tritium and deuterium. This component achieves extremely high temperatures since it receives a high amount of particles (see Fig. 1.6).

Cryostat:

It envelops the reactor using thermal insulators and liquid helium at a temperature of 4 K to maintain the superconductivity of the magnetic coils, which are vital for achieving the high magnetic fields that are needed to confine the plasma. This system also separates the coils from the hottest components of the system (see Fig. 1.7).

Breeding blanket:

Its main function is to get an auto-sustainable production of tritium. It also recovers the energy from the high-energy neutrons inside the reaction chamber, protecting also other components from them. We will

describe this component more accurately in the next section, as it is the place where the reaction that we are studying in this work takes place.

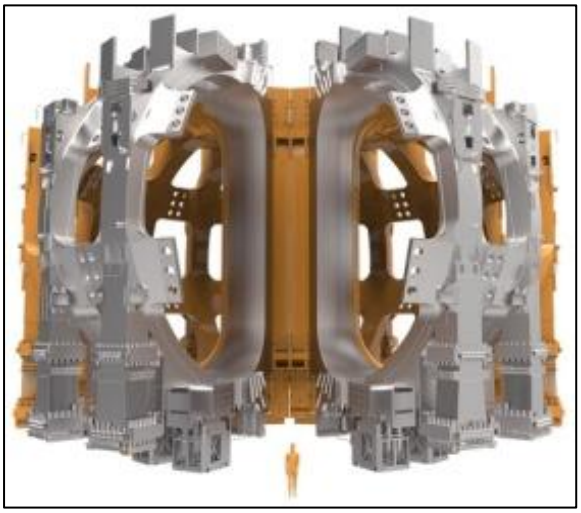

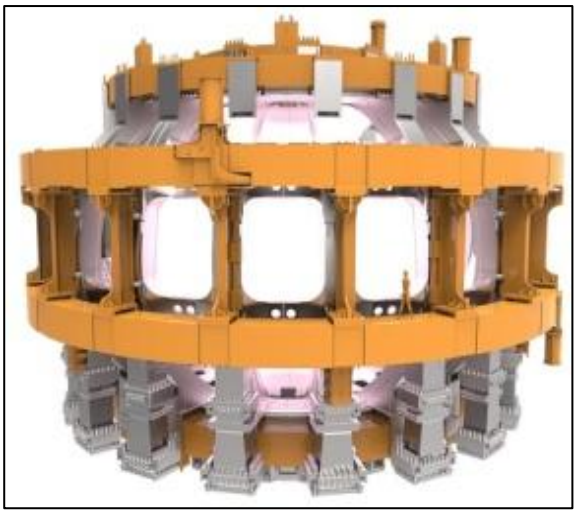

Figures 1.3 and 1.4: Toroidal field system (left) and poloidal field system (right).

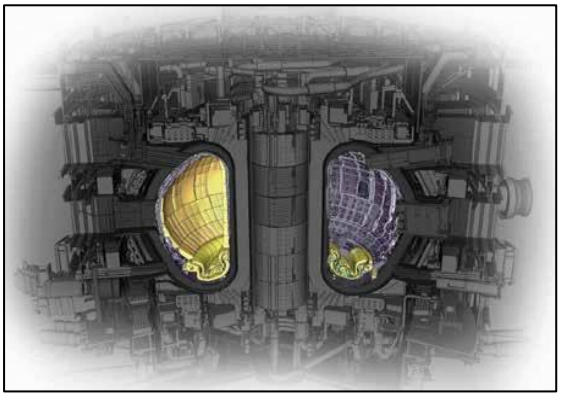

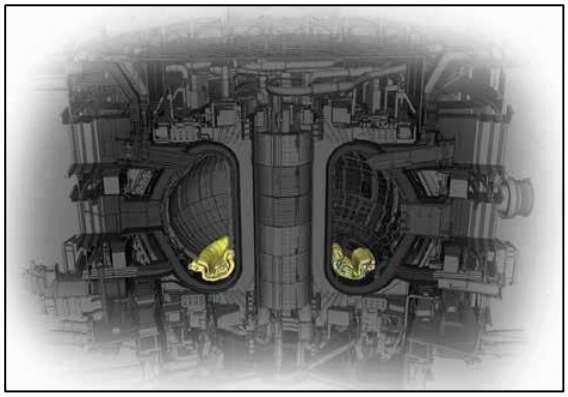

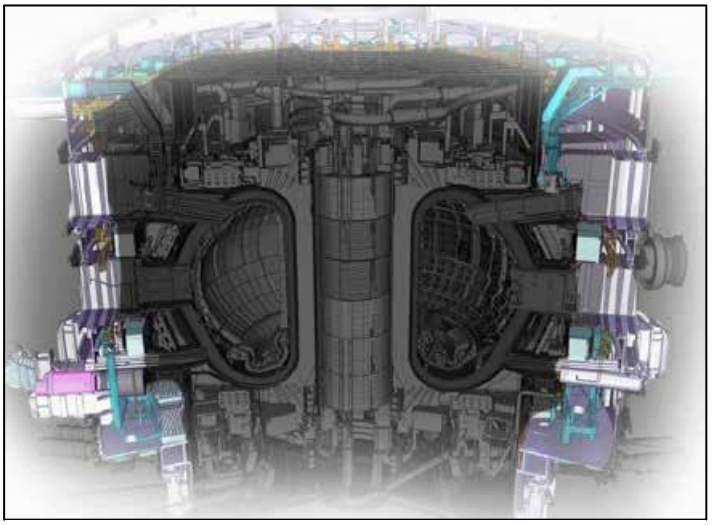

Figures 1.5, 1.6 and 1.7: Respectively from upper left to right and then to the bottom side, the vacuum vessel of the reactor, the divertor, and the tokamak's cryostat.

1.3. The breeding blanket and helium bubbles

The system is made by 440 blanket modules that cover all the walls of the vacuum vessel, protecting the magnets and the steel structure from the high thermal energy and high energy neutrons emitted as a part of the fusion reaction. These neutrons are slowed at the blanket, converting its kinetic energy onto thermal energy. Then, the coolant water collects this energy, producing steam that moves a turbine and generates electrical energy.

The blanket (see Fig. 1.8-1.9) covers a surface of 600 m² and each module measures 1x1.5 m. They consist of one detachable first wall that faces directly the plasma and collects the plasma heat load, and a shield block that provides protection against neutrons.

Then, in order to achieve the needed tritium production for sustaining the reaction (2), the breeding blanket contains lithium based materials. Different materials can be used for this purposes, but the most known ones are the ceramics called Helium-Cooled Pebble Beds(HCPB) or the Li-Pb alloys, which can be cooled by water (Water-Cooled Lithium Lead, WCLL) or cooled by helium (Helium-Cooled Lithium Lead, HCLL). But there is an issue derived from the reaction seen at equation (2). Due to the high temperatures achieved inside the blanket, around 1000K, the lithium and lead components are at a liquified state. This, added to the low solubility of the helium produced and to the high pressures that can be achieved in fusion conditions, makes the helium to nucleate, forming bubbles that are an issue for the efficient work of the breeding blanket.

This last issue is the reason why this work has been developed. Using different simulation methods, a system consisting of a small amount of helium inside an environment of liquid lithium has been simulated, studying the bubble formation at different pressures and analyzing their properties. These include the radius as a function of the pressure, or the critical pressure of bubble formation. Diffusion values were also extracted from the mean squared displacement (MSD) of each atom and their vibration modes using the power spectral density (PSD).

Lithium is one of the materials that are used at the breeding blanket. Other materials like Pb should be used too to run these simulations, but considering that we had enough information to design an effective model using a Lennard-Jones potential, and also that lithium is the simplest of all metals and without enough experimental data from Pb, simulations were made using this material as the liquid medium.

Also, the results were compared with experimental data in order to check if the simulation methods used were correctly describing the relevant physical processes taking place.

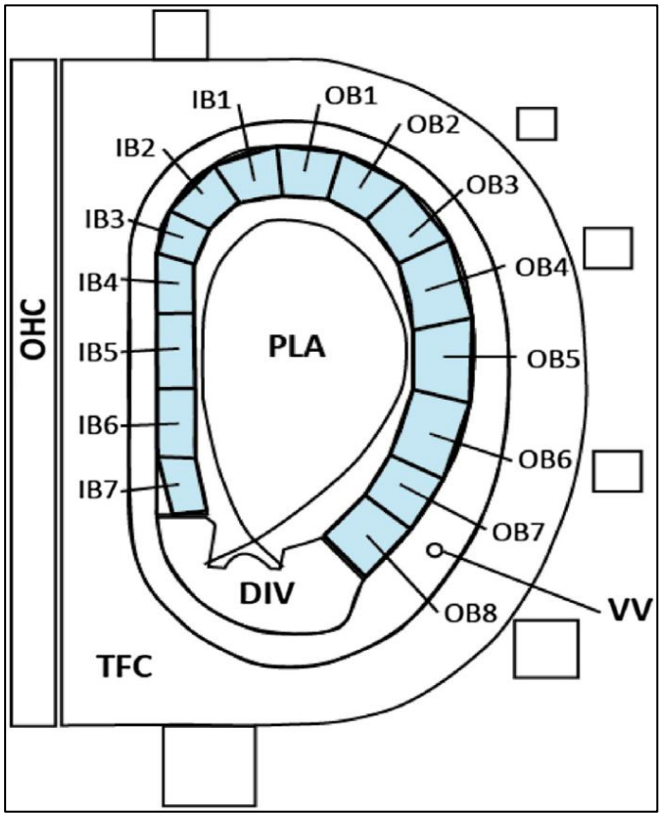

Figure 1.8: Breeding blanket, highlighted in blue. VV is the vacuum vessel, PLA is the plasma, TFC are the toroidal field coils, OHC is the central solenoid and DIV is the divertor. It can be seen that the breeding blanket is divided into modules.

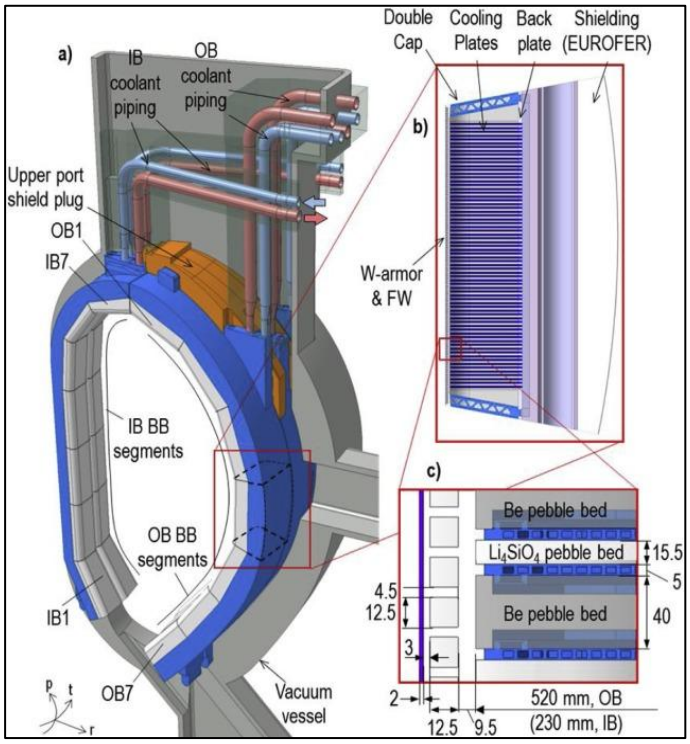

Figure 1.9: Breeding blanket's structure and its refrigeration system.

II. METHODS

2.1. Monte-Carlo simulations

Monte-Carlo simulations are a class of computational algorithms that are used to stochastically explore the phase space of a system and evaluate some of its physical qualities of interest. Using this method, mathematical operations that could be highly complex to solve using algebraic methods can be easily estimated. It can also simulate random actions, like the Brownian motion particles in a gas.

For this purpose, one must generate random numbers. Considering that computers are deterministic machines, one should use suitable algorithms that generate pseudo-random sequences of numbers that depend on an initial seed. Depending on the expression employed, the random number series can be larger and better distributed, providing a better ground for a simulation.

As we know it today, this method was developed in 1940 at Los Álamos by Stanislaw Ulam and John Von Neumann, as part of the research involved around the development of the atomic bomb.

The name of this method comes from the Monte-Carlo casino, one of the biggest ones in the world at that moment, due to the fact that the roulette is considered to be a random number generator.

The algorithm core of this method is the Metropolis algorithm, which implements a Markov chain where every value in a simulation step depends on the previous one. Furthermore, the Metropolis algorithm accepts or refuses iteratively new configurations, comparing their energy to the energy of the previous ones.

In this way, from a system configuration, a random movement of one particle is generated, which leads to a new configuration of the system. The energies of the initial (E_i) and the last configuration (E_F) are computed and compared. In this way:

If $E_i > E_F$ the movement is accepted.

If $E_i < E_F$ then movement is accepted according to a Boltzmann probability distribution:

$$P \propto \exp[\frac{E_i - E_F}{K_B T}] \quad \textbf{(3)}$$

A random number is generated. If this number is larger than the probability, the step will be accepted, but if it is smaller, the step will be rejected.

This method cannot represent the physical evolution in time of a system. This method is meant to describe and sample the equilibrium state of a system (for example the structure of a molecule) but not for a system that evolves during an interval of time.

In order to perform every step, the energy at the current volume must me calculated. Then, a new random volume is generated, from which the energy is also computed. Using then the Metropolis algorithm, the new volume is accepted or not, using for this task a weight guided by the reference pressure.

In this work, the MC simulations have been carried out using 100 millions of

iterations. A pressure control was established spanning the range from 0.1 GPa to 10 GPa. To reproduce the conditions that take place inside the blanket of the reactor, similar values of pressure and temperature have been used. Since the temperature of the blanket can reach 1000 K, we have considered a fixed temperature of 843 K, using pressures of 0.1, 0.2, 0.3, 0.4, 0.5, 1, 5 and 10 GPa and then within a range of pressures between 0.1 and 0.2 GPa in order to study the critical pressure point of the bubble formation.

The system is simulated using a box of 29 A initially and then changing its size as a function of the pressure selected.

The system is simulated using 1000 particles, consisting on 960 lithium atoms and 40 helium atoms.

From these simulations, the radial distribution functions (RDF), the energy and the pressure have been extracted and used to analyze the results.

The RDF is related to the density of the system and describes how it varies as a function of the distance taking a reference particle as the initial point. In other words, it measures the amount of particles that can be found at a distance between r and r+dr from the initial point. If one finds many particles of the same species at short distances, that could mean that nucleation of a bubble is being produced.

The equation that defines this concept is expressed as follows:

$$g(r) = \frac{n(r)}{4\rho\pi r^2 dr} = \frac{n(r)}{n_{id}(r)} \quad \textbf{(4)}$$

Where the average density of particles is expressed as ρ=N/V, $n(r)$ is the mean number of particles that are at a distance between r and r+dr, and $n_{id}(r)$ is the value of this number in an ideal gas.

We have computed the RDF for all three interatomic interactions: He-He, Li-Li and He-Li, using both MC and Molecular Dynamics (MD).

2.2. Molecular dynamics simulations

Introduced by Alder and Wainwright for the study of hard-sphere interactions [11], this model aims for the resolution of the Newtonian equations of motion over a time range divided in intervals. The integration method used is the Verlet-Leapfrog algorithm, which conserves the energy of the system.

In the MC algorithm, unlike in MD, the pressure is stabilized using a barostat, keeping the temperature fixed at a given value. For this matter we add a thermostat.

The MD method allows us to implement Berendsen's barostat and thermostat [12], [13]. This allows achieving what it is called the NPT collectivity, where the number of particles, the pressure and the temperature of the system remains constant. Since the temperature of the system is obtained from the kinetic energy at the MD method and it changes with time, we evaluate it from the expression:

$$T(t) = \sum_{i=0}^{N} \frac{m_i v^2{}_i(t)}{K_B N_F} \quad \textbf{(5)}$$

Where N_F=3N-3 is the number of degrees of freedom of the system.

This is explained as follows. For a set of particles N moving in a 3-dimensional space, the number of degrees of freedom (DF) will be:

$$DF = 3N - k \qquad \textbf{(6)}$$

Where k is the number of constraints of the system, 3 for our situation.

In the Berendsen's thermostat one multiplies equation (5) by a corrective factor λ, which is expressed as:

$$\lambda = \sqrt{1 + \frac{\Delta t}{\tau_T}\left(\frac{T_{REF}}{T} - 1\right)} \quad \textbf{(7)}$$

Furthermore, in the MD method, the pressure is controlled by multiplying the box length by a factor μ that makes the box to change its size. If we imagine this system as a box filled with a certain number of particles, by changing the box's dimensions we can control the pressure of the system. This factor μ is expressed as follows:

$$\mu = \sqrt[3]{\left[1 + \frac{\Delta t}{\tau_P}\beta_P(P - P_{REF})\right]} \quad \textbf{(8)}$$

Where β_P is the compressibility of the system, Δt is the integration time step, τ_P and τ_T are free constants, P is the pressure and P_{REF} is the pressure at which we want the system to stabilize.

The MD simulations using this method were carried out using 60000 steps considering a time interval of 2 fs between consecutive time points. A pressure scan was made in the range from 0.1 to 10 GPa as it was done with the Monte-Carlo method before.

All simulations were done at a fixed temperature of 843 K.

On both methods the energies of the system, the pressures and the radial distribution functions were represented, but in the MD simulations the spectra was also tracked. This latter quantity is obtained from the velocity autocorrelation function (VAF). Mean squared displacement (MSD) was also computed, which measures the deviation of the position of a particle with respect to a defined reference position over time.

If we look follow the mathematical trajectory of an atom in a liquid is, we readily notice that it moves following a series in a Markov chain.

If we set the example of an atom's displacement along a 1D axis, considering that the atom has the same possibilities of going forward or backwards, the mean displacement will always be 0. But, if we compute its squared value, the displacement will be always positive, thus allowing to obtain a better idea of how far the atom has travelled.

For that matter, the Mean Square Distance (MSD) is defined as it follows:

$$MSD = \langle|\vec{r}(t) - \vec{r}(0)|^2\rangle \quad \textbf{(9)}$$

When representing the values obtained from this parameter, it first appears a transient state, but at long term, it is followed by a steady state. If we measure the slope of the MSD as a function of time for large times, which will also be the limit of the MSD when $t \to \infty$, we can obtain the diffusion coefficient D of helium and lithium by using the Einstein equation:

$$\lim_{t\to\infty} MSD = 6Dt \quad \textbf{(10)}$$

The velocity autocorrelation function (VAF) describes how the velocities change as a function of time. It is expressed as follows:

$$V(t) = < \vec{v}(t) \cdot \vec{v}(0) > \quad \textbf{(11)}$$

Where brackets indicate averages over time intervals and over all particles in the system. For an isotropic system, the equation can be expressed as follows:

$$\lim_{t\to\infty} V(t) = \lim_{t\to\infty} < \vec{v}(t) \cdot \vec{v}(0) > = <v2>=0 \quad \textbf{(12)}$$

Using the VAF obtained from the simulations, we can obtain the power spectrum, S(ω), by taking its Fourier transform.

The power spectrum detects the main vibrational modes of a system, including the values that are under 100 ps^{-1}, which are related to rotational and translational modes. On the other hand, vibration frequencies around and above 500 ps^{-1} are related to stretching and bending vibrations.

2.3. Potential models

A pairwise Lennard-Jones potential was used to model the atomic interactions between He-He particles (see Fig. 2.1). The Lennard-Jones has a parameter σ which is the value of the finite distance at which the potential value is 0, and a second parameter ϵ that defines the maximum depth of the interaction. Furthermore, it depends on r_{ij}, the interatomic distance between particles i and j. The LJ potential reads as follows:

$$U_{LJ} = 4\epsilon[(\frac{\sigma}{r_{ij}})^{12} - (\frac{\sigma}{r_{ij}})^{6}] \quad \textbf{(13)}$$

The first term inside the brackets describes repulsion at short distances, while the second one describes attraction when the particles are far apart from each other.

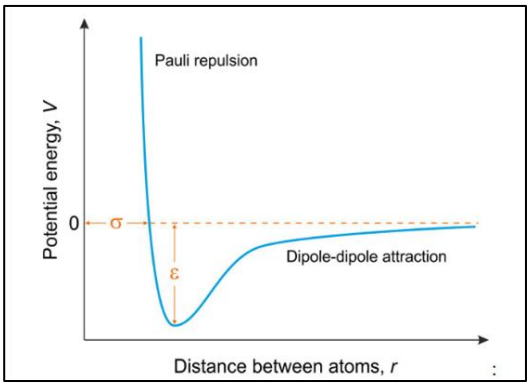

Figure 2.1: Interatomic Lennard-Jones potential.

When the two atoms are separated, the most relevant part of the attraction that takes part is the dipole-dipole interaction. Once the particles approach, they tend to move to a more stable steady state, with the lowest possible energy which implies that the inter-particle distance is somewhere around r_σ. Then, as both particles continue their approximation, the energy starts rising due to the Pauli repulsion.

This potential has been used to describe the interaction between each pair of particles, and therefore it has also been used to evaluate the energy per particle. In this way, one chooses a particle and computes the interactions with all the other atoms of the system. Then one moves to the next particle and does the same thing, but skipping the interaction with the previous particle. This process is repeated till all pairs of particles have been measured. When done, this provides a direct measurement of the potential energy of the system.

In our simulations, three different potentials have been used,

corresponding to the Li-Li, He-He and He-Li interactions.

The Li-Li potential was modeled as follows (the values of the parameters are added in the appendix part):

$$V_{Li-Li}(r) = \frac{a_0}{r^{12}} + a_1 \exp(-a_2 r)\, cos(a_3(r - a_4))$$

(14)

On the other hand, the He-Li interaction can be modeled by a LJ potential, as it will be explained below. For the He-He potential, the expression is the same as in equation (13).

The Li-He potential is also of the Lennard-Jones type, but with mixed parameters and cutoff at a given distance (σ_{He-Li}).

For the Li-Li interaction, σ and ϵ were extracted from Canales et.al. [1], set at 843 K.

At the simulations the potentials were measured in Kelvins (K) and the distances in Angstroms (A).

The parameters chosen for both simulation methods were the next ones:

$\sigma_{He\text{-}He}$=2,5560 A

$\sigma_{Li\text{-}Li}$= 2,5668 A

$\epsilon_{He\text{-}He}$= -800 K & -1200 K

$\epsilon_{Li\text{-}Li}$= -888 K

The Lorenz-Berthelot rules were used to obtain the parameters for the He-Li interaction. The σ parameter is calculated as:

$$\sigma_{He-Li} = \frac{\sigma_{He}+\sigma_{Li}}{2} \quad \textbf{(15)}$$

Using a value of 2.5615 A, according to the parameters chosen. In much the same way, the ϵ parameter is given by the expression:

$$\epsilon_{Li-He} = \sqrt{\epsilon_{He-He}\epsilon_{Li-Li}} \quad \textbf{(16)}$$

With a numerical value that depends on $\epsilon_{He\text{-}He}$. We have found:

-842 K if $\epsilon_{He\text{-}He}$ = -800 K

-1032 K if $\epsilon_{He\text{-}He}$ = -1200 K

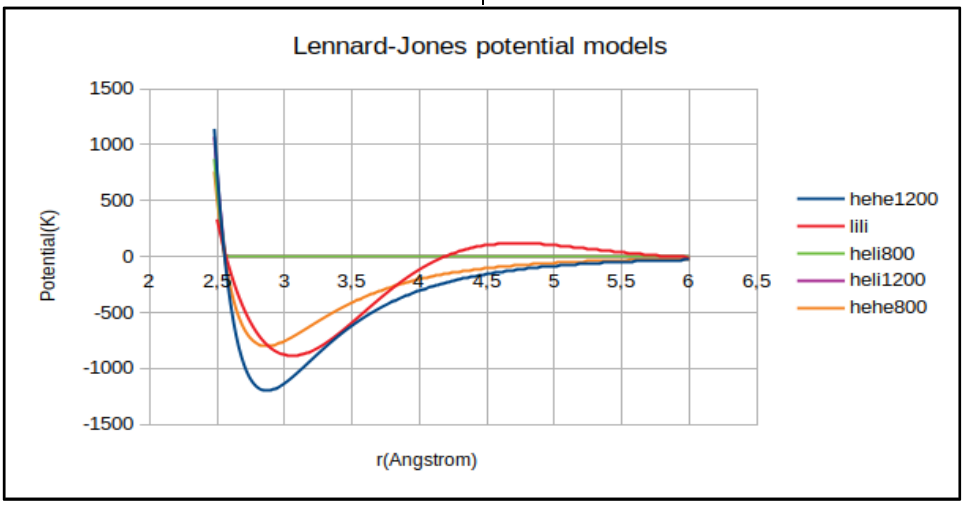

Figure 2.2: Lennard-Jones representation of potential models used.

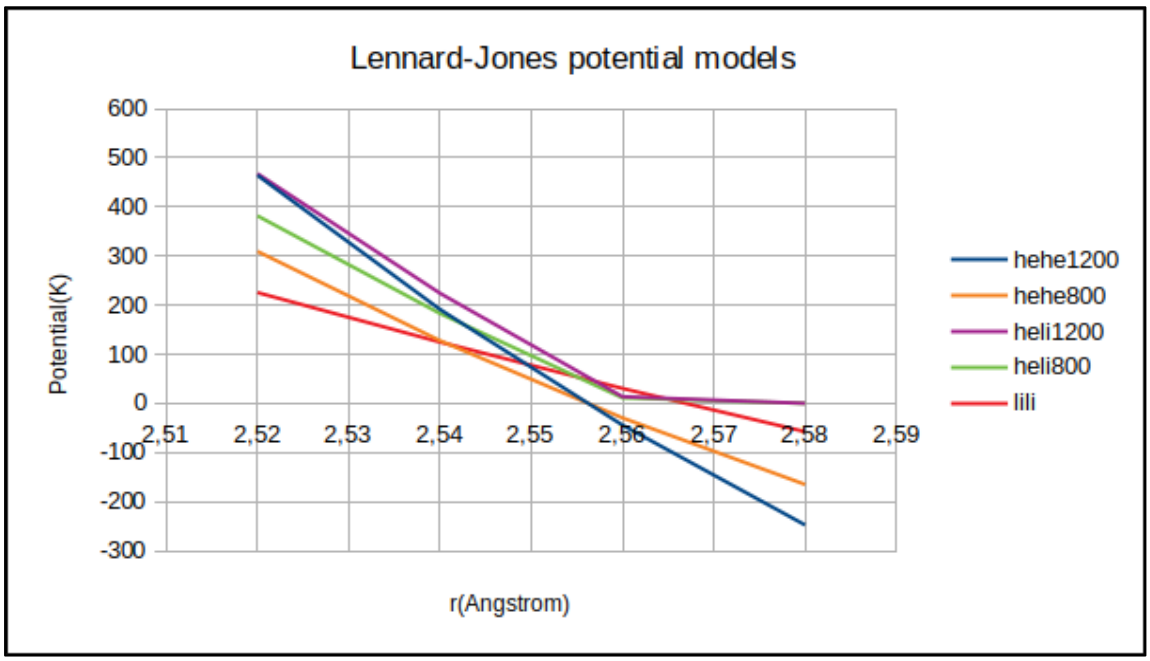

Figure 2.3: Lennard-Jones potential models used zoomed at their crossing zone.

The form of the potentials is reported in Figs. 2.2. and 2.3. As it can be seen, the He-Li interaction is weaker than the interaction between particles of the same atom. This means that the formation of pairs of different species is quite unlikely, unless special conditions are met. This will lead to the formation of bubbles of helium once we increase the pressure, as it will be seen later.

This is what happens when we show the He-He and Li-Li interactions at figure 2.2. Helium tends to interact with other helium particles more easily than lithium does with other lithium particles, but only if we choose the -1200 K potential for ϵ. For the -800 K model, the interaction is stronger on the Li-Li model.

All this means that finding clusters or helium bubbles is favoured if the required conditions of pressure and temperature are applied.

However, considering how weak the interaction between helium and lithium atoms is, if enough low temperatures are applied to a He-Li mixture, clusters can be generated. These structures will be mostly composed by a lithium atom surrounded by helium atoms. This structure would consist, in theory, of a lithium atom surrounded by a helium bubble.

For example, Portos et.al. [2] showed that while having temperature conditions near 0 K, He-Li clusters could be formed.

However at the temperatures and conditions at which we are working, around 1000 K, and with a medium that is mostly composed by lithium atoms, these structures will not be possible, and then the model of a helium bubble in a lithium bath will prevail.

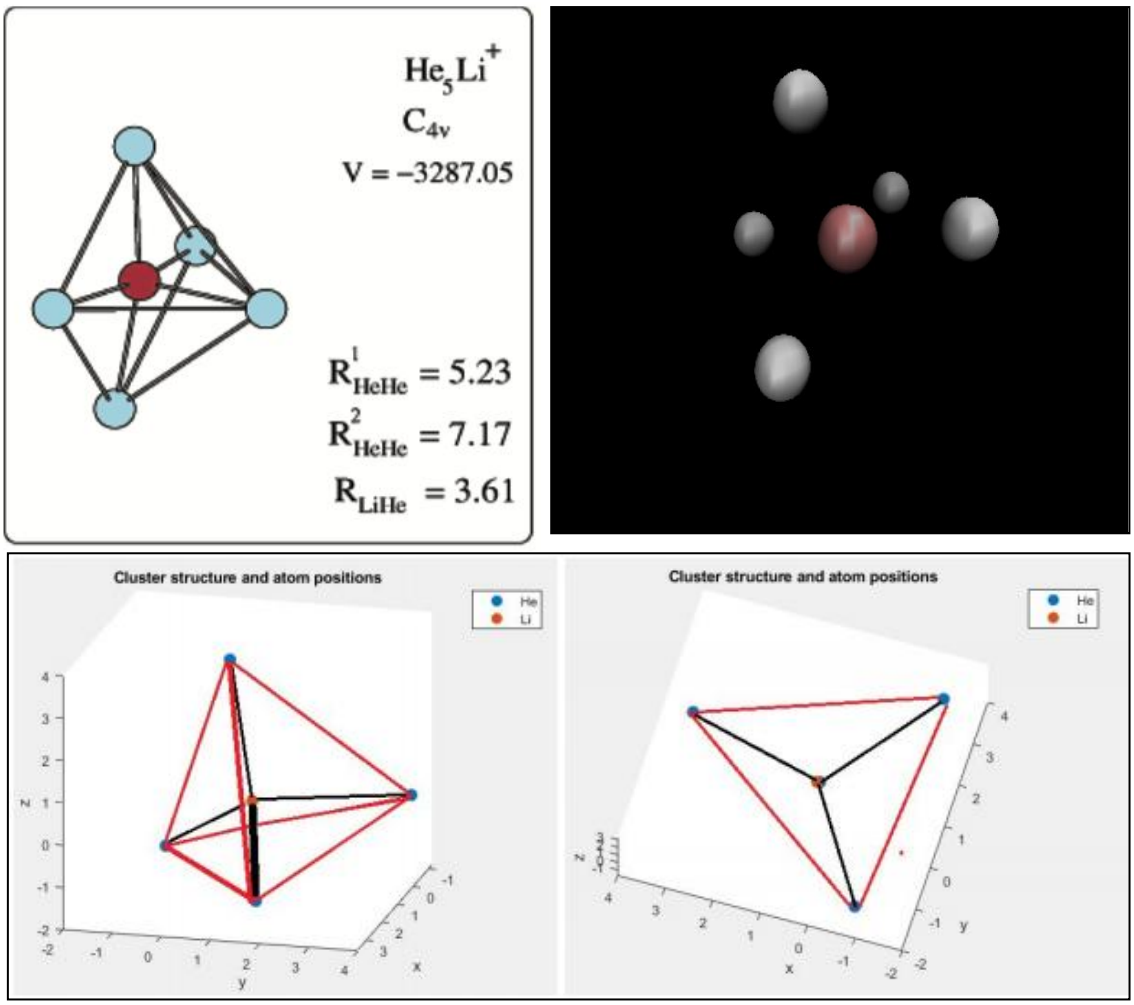

Figures 2.4, 2.5 and 2.6: Upper left, He-Li cluster model described by Di Paola et.al. [10]; upper right, simulated He-Li cluster model run by Portos et.al. [2] at 10 K; bottom part, simulated He-Li cluster model using Matlab consisting of 4 helium atoms and 1 lithium atom at the center, forming a pyramid-like structure. Even considering that the described model at figure 2.4 uses a +1 charged lithium, the model also fits well with Portos et.al. [2] simulation. The model of the figure 2.6, even without considering this charged atom, it still forms a clear pyramidal structure. This last model was simulated at a temperature very close to 0 K, but computing all interaction potentials using equation (13).

III. RESULTS

3.1. MC and MD comparison

Pressure

First of all, it is necessary to know how the pressure evolves during the simulation. We must keep this value is fixed using an external mechanism, such that the pressure fluctuates around this value. This is because the pressure is not fixed as is the temperature, in the MC method, so it will fluctuate even if we are correcting as it was explained in chapter II. So, if everything goes as expected, this value should always take values that are close and move around the pressure we have fixed in the simulation. This is something that must be checked as the simulation goes on, and can be taken as a test to what we are doing.

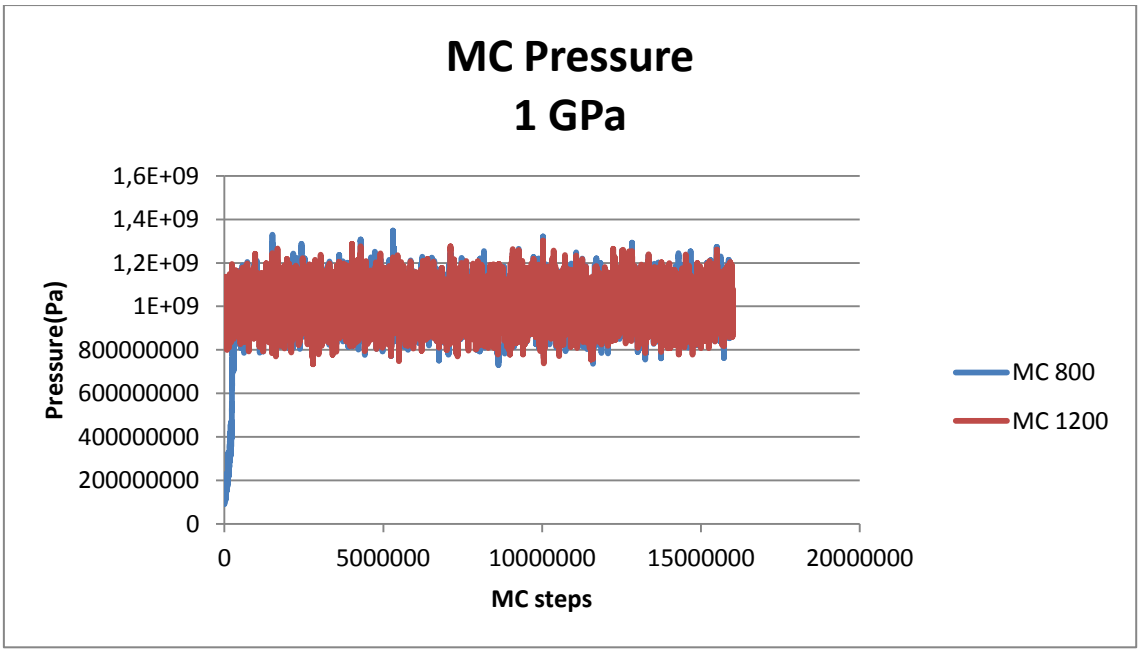

Figure 3.1: Evolution of the system's pressure at 1GPa for MC method at epsilon=-800 K and -1200 K till 16 million MC steps.

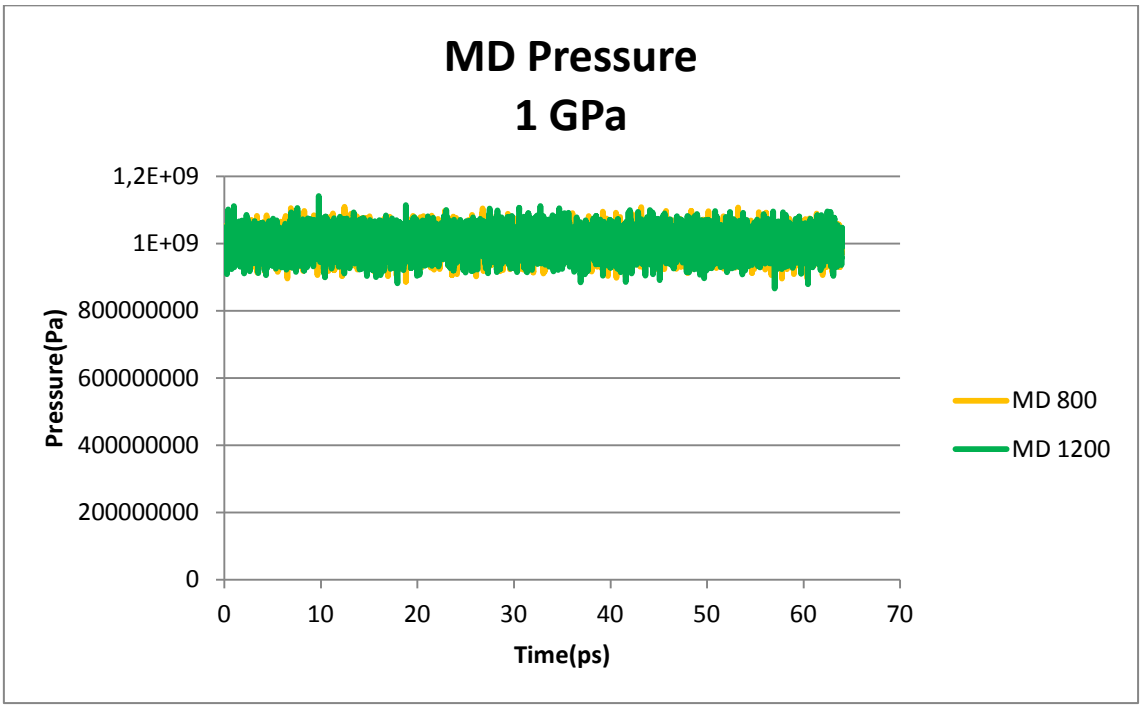

Figure 3.2: Evolution of the system's pressure at 1GPa for the MD method at epsilon=-800 K and -1200 K till 64 ps (32000 MD steps).

Figures 3.1 and 3.2 show the evolution of the pressure along two different simulations. As it can be seen, the pressure really fluctuates around an average value, which indicates that everything is proceeding as expected. After an initial transient time, pressures for both potentials and methods grow to the value that we have fixed externally, in this case 1 GPa, and keep fluctuating around this value.

As we can see, the different methods make the fluctuations be different in each case. The MC fluctuations are two times larger than the MD ones.

By other part, the pressures stay completely unaltered for both potentials, meaning that the only visible change is produced between the two simulation methods. As we can see, MC pressure fluctuations are larger than the ones produced using MD. However, these fluctuations are around the designed pressure value.

Energy

After the pressures, we can proceed to analyze the evolution of the energy of the system.

The energy was computed at the simulations by adding the contribution of all pairs of particles to the potential energy, plus the constant term proportional to the temperature, which corresponds to the classical expression of the kinetic energy:

$$E_K = \frac{3NK_BT}{2} \quad \textbf{(17)}$$

Where K_B is the Boltzmann constant, T the temperature and N is the number of atoms.

Being the total energy of the system expressed as:

$$E_{TOT} = E_{POT} + E_K \quad \textbf{(18)}$$

If everything goes as expected, the system's energy should start at high values due to the fact that the initial system is in a random configuration that is energetically unfavorable. Then, it should descend to lower values, as the system is evolving to an energetically favorable distribution which means that the simulation is working exactly as we expected it to work.

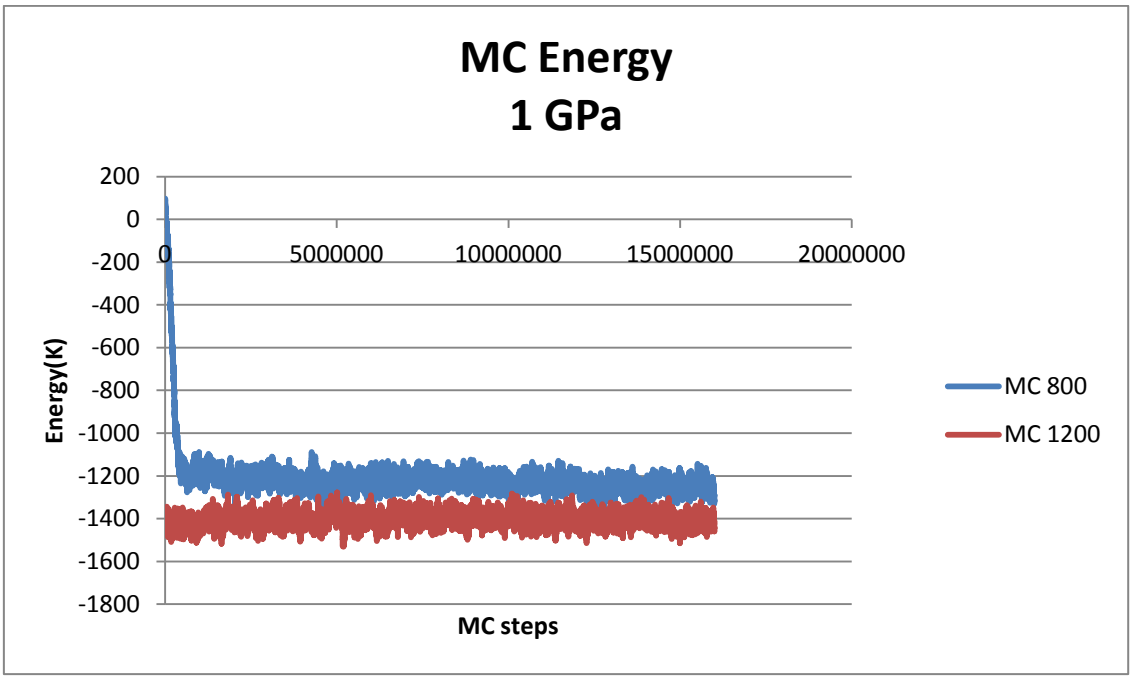

Figure 3.3: Energy evolution of the system for the MC method and for epsilon= -800 K and -1200 K till 16 million MC steps.

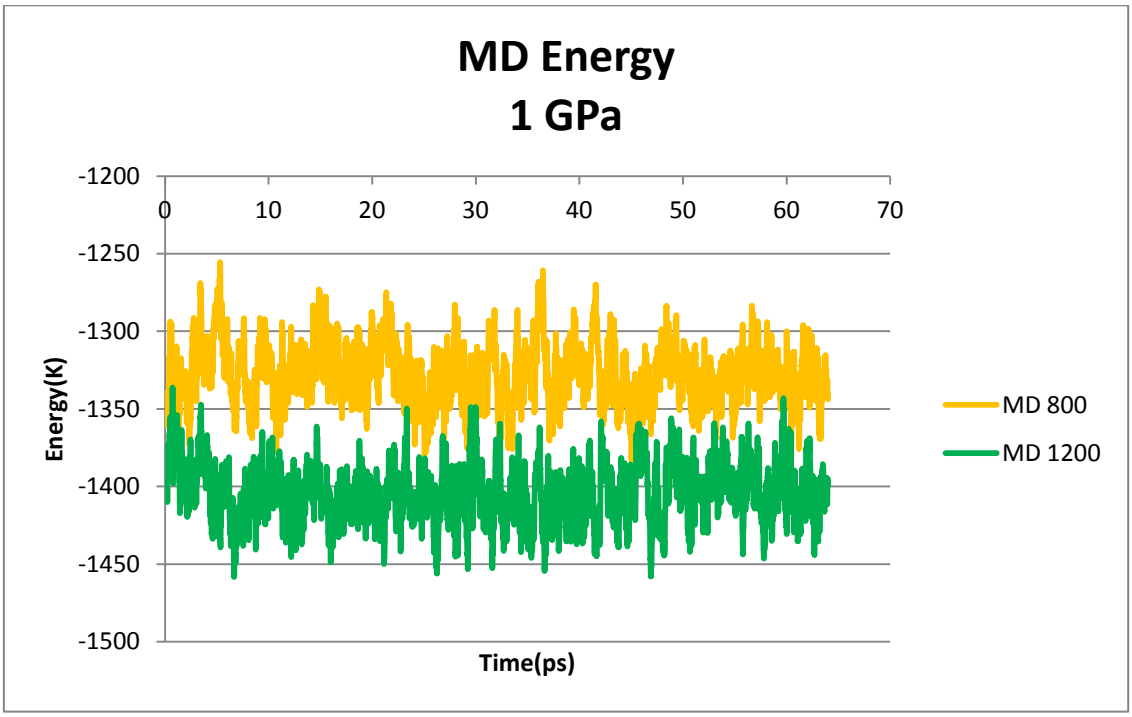

Figure 3.4: Energy evolution of the system for the MD method at epsilon=-800 K and -1200 K till 64 ps (32000 MD steps).

As we see from figures 3.3 and 3.4, the energy of the system tends to an stationary value already at the very beginning. This means that the system indeed evolves to an energetically favorable configuration, where it finds a stable steady-state that fluctuates around a determinate energy value. This value corresponds to the less energetic system's configuration that has been found, meaning that the system has arrived to a stable configuration.

The final steady-state energy is very similar in both methods. If the chosen ϵ is -1200 K, the final energy would be lower than if ϵ was -800 K.

Fluctuations in the MC method are again higher than in the MD method, as we saw previously with the pressure. If we look then at their steady-state energy values, we see that they are very similar, specially when using the -1200 K potential, although we can see that the average values of the fluctuations of MD and MC are closer than in the -800 K potential.

Radial distribution function

The radial distribution function (RDF) sheds more light about the structural properties of the system, and how particles are distributed inside the box.

Figure 3.5 shows us the RDF of the Li-Li interaction using both simulation methods and both potentials of -800 K and -1200 K. The results indicate that both algorithms, MC and MD agree perfectly and give almost the same RDF. Moreover, both potentials agree perfectly in this model, giving also the same RDF.

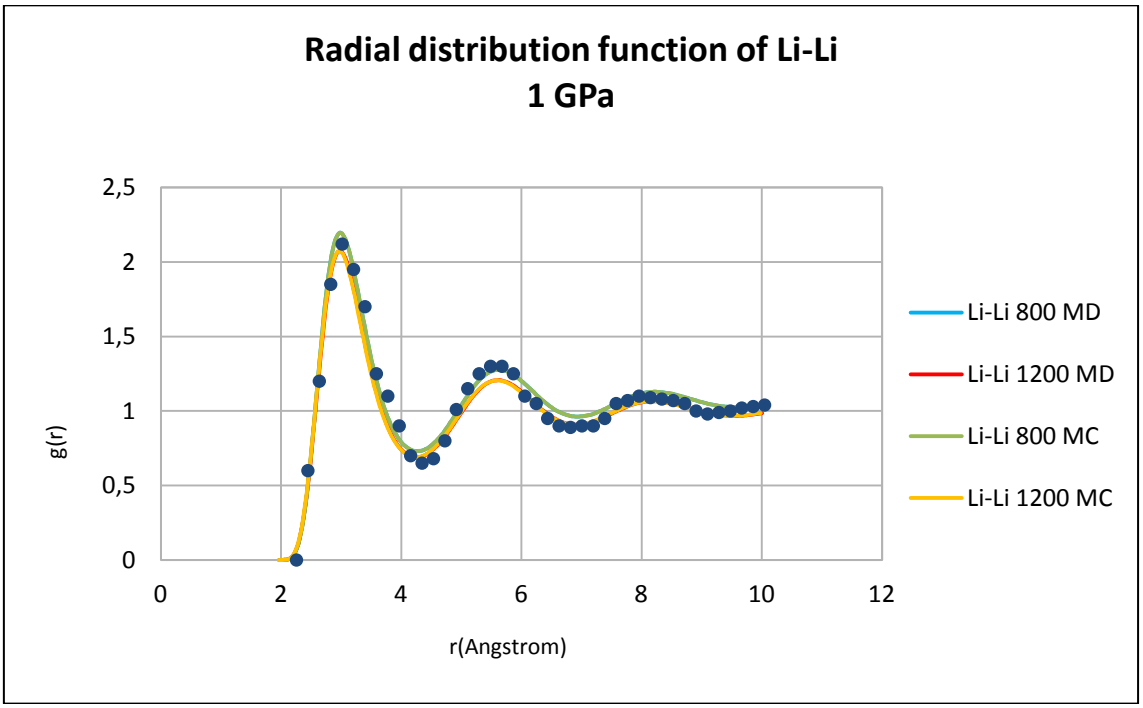

Figure 3.5: RDF of Li-Li interaction including the experimental data from Canales et.al. [1]. All of these RDF have been computed at 843 K.

The plot also shows an RDF model for the Li-Li interaction obtained by Canales et.al. [1] at the temperature of 843 K and 1 GPa. This model matches very well with our simulation, especially at the maxima and minima positions, thus showing that the Li-Li interactions are quite consistent with the ones we use in our model, and that they work well for this simulation.

The model proposed by Canales et.al. [1] was in good agreement with experimental data for the static structure factor S(k) at 470 K. Considering that our model for the Li-Li interaction is the same, we will assume that it can correctly model the structure of Li at 843 K, although to be sure we would need experimental results at this temperature, that are currently lacking.

For all these reasons, from now on we focus mainly on the MC results and work with the potential of -1200 K. It should be pointed out that this potential was designed to check if the helium bubble could be stable at 0.1 GPa, but as we could see later, that is not the case. However, considering that the energies computed were slightly lower for this potential, as it was seen in figures 3.3 and 3.4, and also that it makes the system be more stable, we decided to keep it in our analysis.

3.2. Study of the helium bubble formation

Li-Li radial distribution functions

The RDFs of Li-Li, He-Li and He-He interactions were obtained and analyzed at different pressures in the range from 0.1 to 10 GPa. The computed pressures were 0.1, 0.2, 0.5, 1, 5 and 10 GPa.

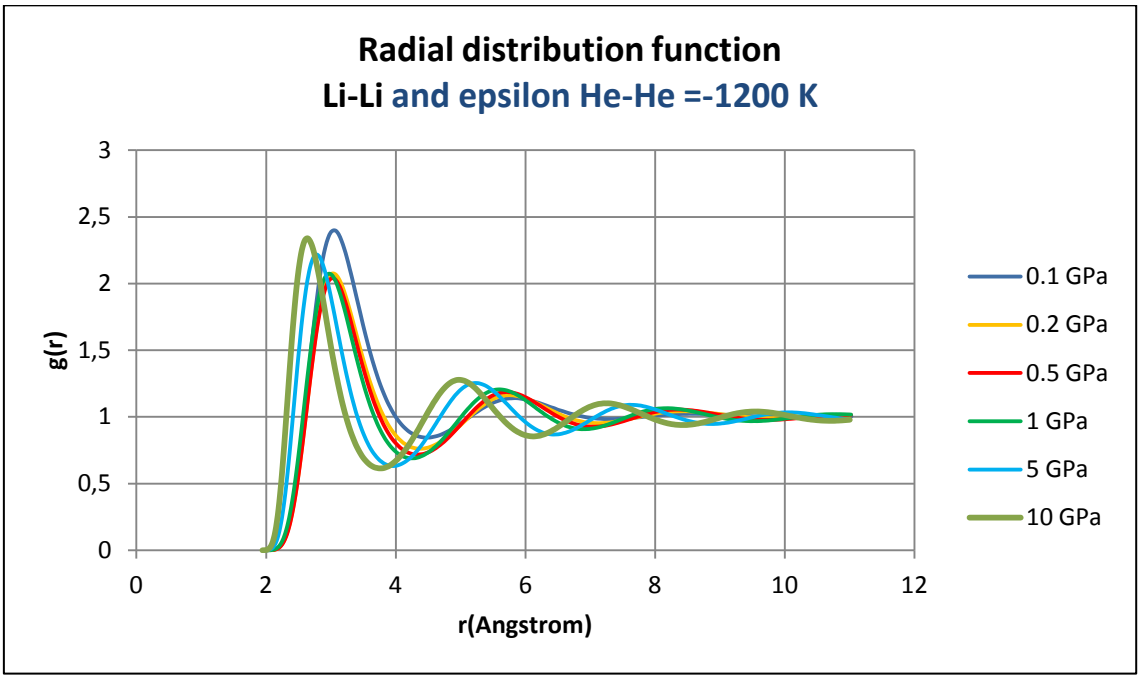

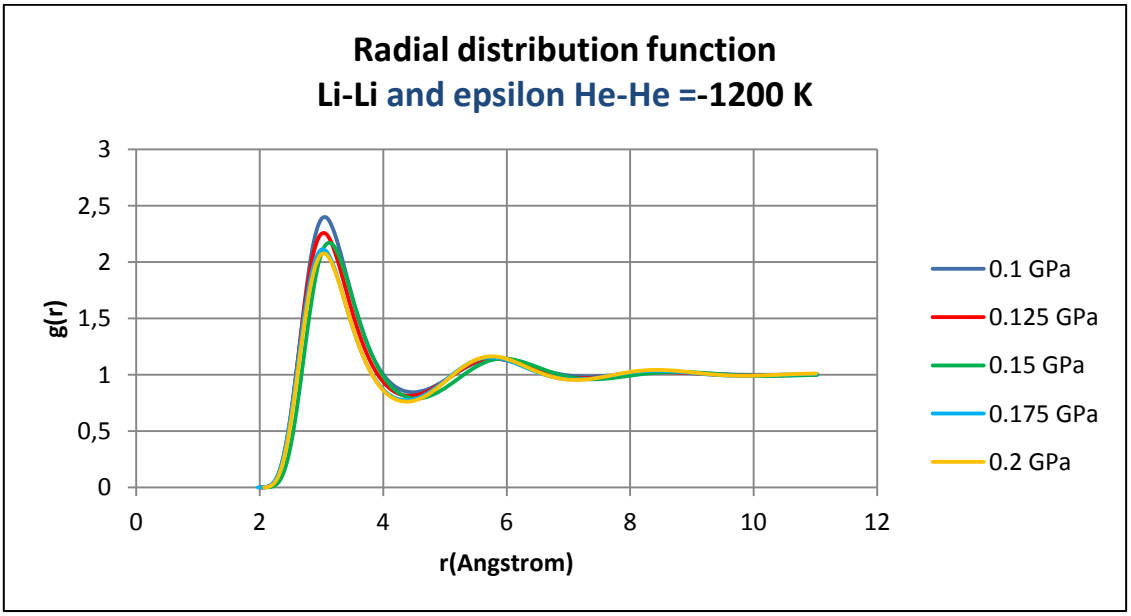

Figures 3.6 and 3.7: RDF of Li-Li interaction for a range of pressures between 0.1 and 10 GPa. The bottom plot shows the RDF of the Li-Li interaction for the range of pressures between 0.1 and 0.2 GPa.

Figures 3.6 and 3.7 show the RDF of the Li-Li interaction at different pressure ranges, from 0.1 to 10 GPa, and in the more reduced interval that goes from 0.1 GPa to 0.2 GPa. These two intervals were properly divided in intermediate pressures, which were 0.1, 0.2, 0.5, 1, 5 and 10 GPa, and 0.1, 0.125, 0.15, 0.175 and 0.2 GPa, respectively. This allows us to have a general view of how the system behaves at small and large pressures and also to see what is happening between 0.1 and 0.2 GPa. This is due to the fact that the

critical bubble formation pressure seems to be between these two values. The latter interval is of most interest as the critical bubble formation point seems to lay inside it.

The RDF from these figures shows us the lithium medium that surrounds the helium bubble. It is proportional to the number of lithium particles that are at a distance between r and r+dr from the initial point, as we explained before.

As it can be seen, there is an initial ordering and a periodicity, but the amount of particles that can be found as the distance increases is reduced. This is due to the ability of atoms to move in a fluid in a dynamic way, and thus fluids do not maintain a constant structure and lose all this structure at long distances.

Considering then that we are using LJ models here, the first peak will appear at a distance similar to σ, which indicates the first coordination sphere of the liquid. As long as the distance from the reference particle increases, lower peaks will appear at intervals of a distance similar to σ between them, till the particles become independent one of each other, returning the distribution to the homogeneous value g(r)=1. Still, we need then more information if we want to know how helium bubbles are being formed.

He-Li radial distribution functions

As shown in figure 3.8, its shape is very similar to the one that corresponds to a gas. The main difference is that the RDF of a gas is quite smooth, with peaks that are either absent or of very low strength. This is due to the repulsion that exists between helium and lithium atoms, as it was seen in figures 2.2 and 2.3, when Lennard-Jones model was explained. As it was seen, a huge difference between the shape of the same atom potentials (He-He and Li-Li) and the He-Li potential appeared.

This changes at 1 GPa, when we can see that the first peak is significantly larger than the first peak seen at lower pressures.

At 5 GPa, peaks are clearly defined, which means that aggregates of helium and lithium are clearly formed. Even considering that these aggregations are already formed at 1 GPa, they should be better defined when the system pressure reaches 5 GPa.

Looking at figure 3.9 we see what happens between 0.1 and 0.2 GPa. We see that at 0.1 GPa the RDF curve is almost flat, only at the beginning it shows a little depression, achieving the bulk density as r tends to infinite.

When the pressure increases, we see how the first peak decreases its intensity, increasing the slope of the curve. This is similar to the 0.5 GPa case analyzed before, which shows a curve that is similar to the 0.2 GPa one, but with better defined peaks. The 0.5 GPa first peak also starts increasing, forming later the sharp first peak of the 5 and 10 GPa curves.

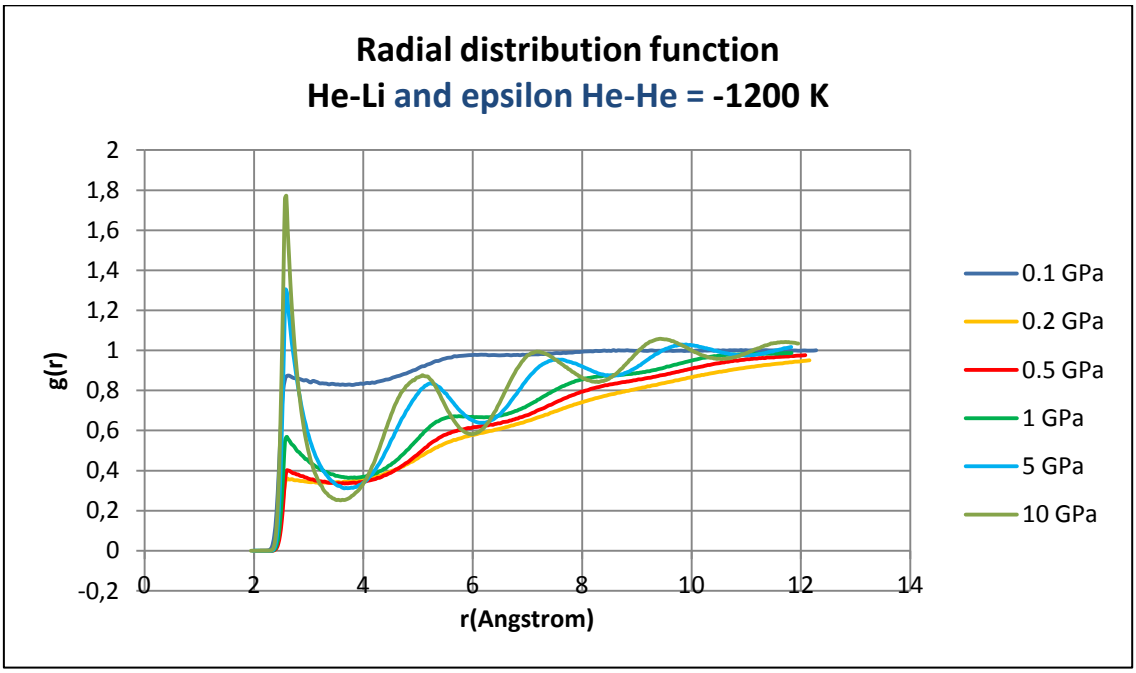

Figure 3.8: RDF of the He-Li interaction for the range of pressures between 0.1 and 10 GPa.

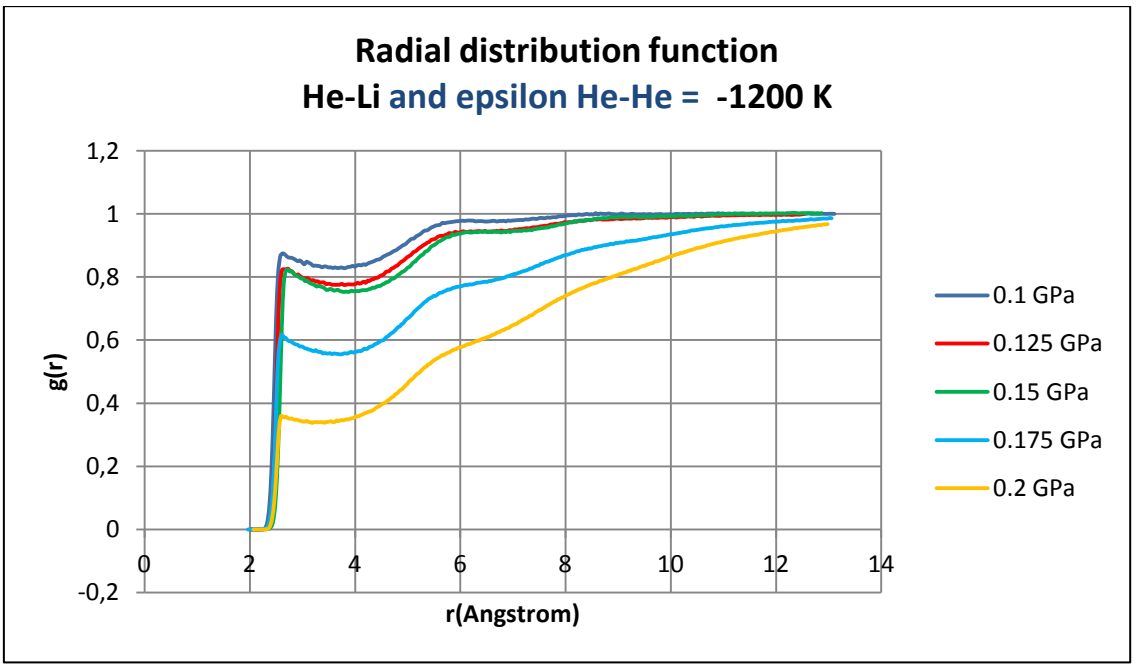

Figure 3.9: RDF of the He-Li interaction for the range of pressures between 0.1 and 0.2 GPa.

He-He radial distribution functions

At this point we already have an idea of the pressure values at which helium bubbles are being formed. In the following we want to check that they are in fact formed, and find out at which pressure starts their nucleation.

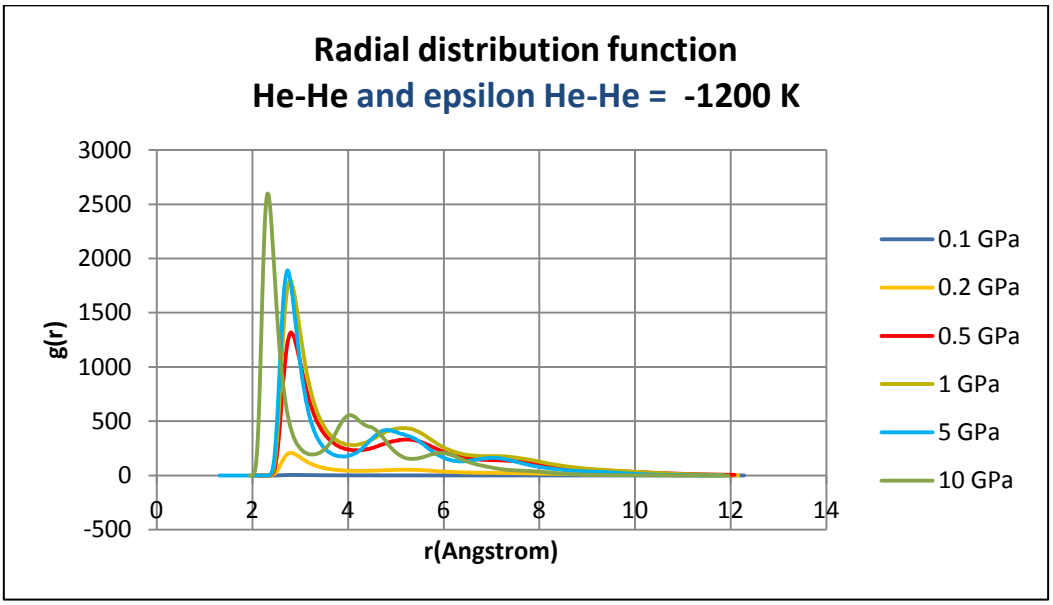

Figure 3.10: RDF of the He-He interaction at the pressure range from 0.1 to 10 GPa.

As can be seen by looking at figure 3.10, two clear peaks are being formed from 0.5 GPa in advance, but we can appreciate even a second peak at 0.2 GPa, although this peak is very flat.

The appearance of these peaks indicates the formation of bubbles, as seen from a largest peak at short distances. After it, the following peaks tend to decrease when r is increased, until they reach the asymptotic value g(r) =1. If the system was a solid, the peaks should be equal or at least similar for large r, meaning that a periodicity is sustained along the medium. It is not the case for this example. There are large peaks that are neither periodic nor of equal intensity, and this is because particles can move in the medium, as opposed to what happens in a solid, where atoms oscillate around their equilibrium positions.

We start to see then bubble formation at 0.2 GPa, but an acceptable stability of these bubbles should be reached at 0.5 GPa, even considering that at 1 GPa the bubble stabilization would reach a better state, nearly the same than the one that is reached at 5 GPa pressure.

When the pressure is increased to 10 GPa, then the peaks become sharper and the density increases, meaning that the bubble gets more and more compact if pressure is raised.

Therefore, the critical pressure for bubble formation should be under 0.2 GPa, since we do not find bubbles at pressures as low as 0.1 GPa. For this reason, a more detailed scan in range from 0.1 to 0.2 GPa was done, using the previously used values for the other RDF simulation graphs.

According to figure 3.11, we have indeed two peaks at 0.2 GPa, but it seems that there is a small one at 0.175 GPa, together with a second very flat peak.

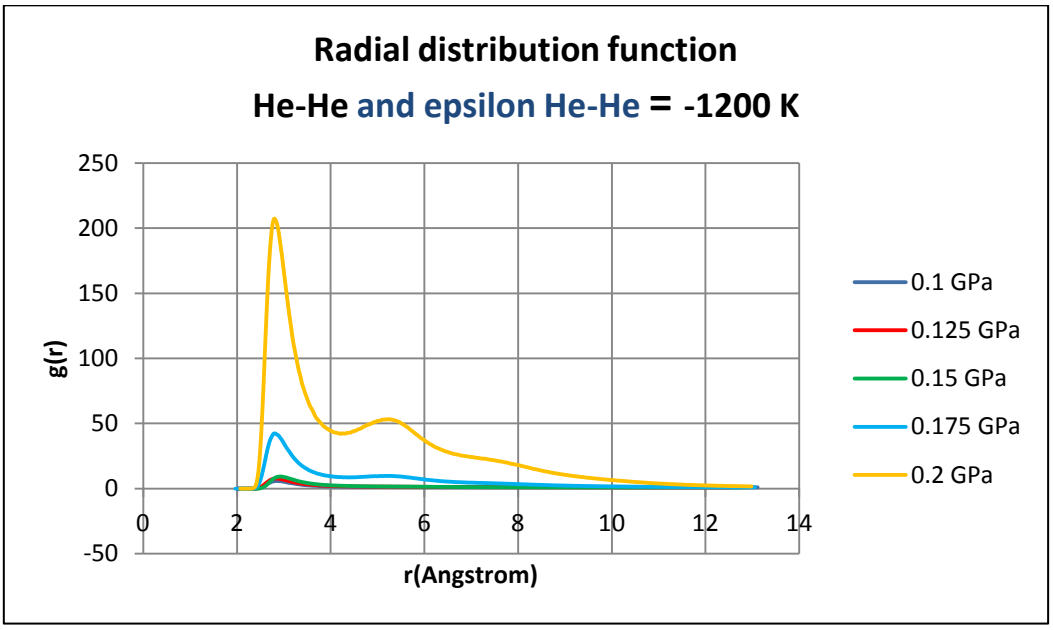

Figure 3.11: RDF of the He-He interaction at the pressure range from 0.1 to 0.2 GPa.

This means that there is bubble formation at 0.175 GPa, but not at 0.15 GPa. We see a remarkable height difference between both peaks, meaning that if for some reason there is some helium aggregation at 0.15 GPa, it is not enough to form a bubble.

Then, for this reason we can conclude that the bubble formation starts at some value under 0.175 GPa, and reaches a stable point at the value of 0.5 GPa, even considering that at this value the bubbles formed are still not good compacted as the ones formed at 1 GPa. However, these bubbles can reach much better stability and compactness at values of 5 and 10 GPa, specially at this last value, where we can appreciate a significant growth of the RDF value and a sharper peak.

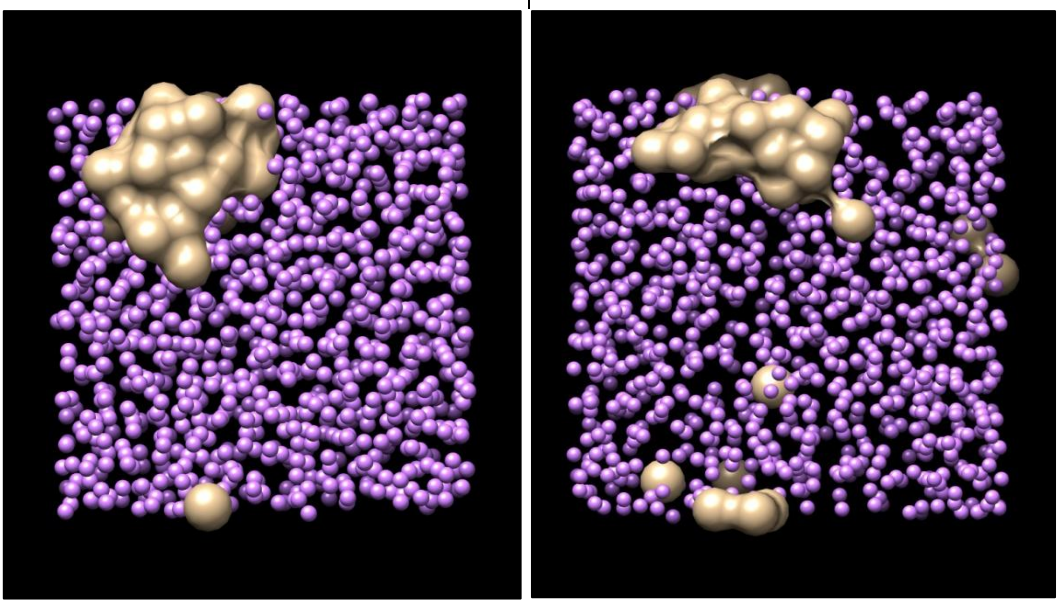

Figures 3.12 and 3.13: From left to right and from up to down, images from the helium nucleation at pressures of 0.2 and 1 GPa, respectively.

Figures 3.12 and 3.13 confirm all that. If pressure is increased to 0.2 GPa, like in figure 3.12 appears, we can see how an aggregate is formed. However, it is clearly seen that this aggregate does not have a regular shape, which could suggest that the aggregate is not stable (by definition and with all forces acting equally distributed around the bubble, the less energetic configuration that must be formed should be the sphere). This matches with what was said before, that even in the case when aggregations are formed, they would be still not stable, and also we can see that they could be not even well defined because the aggregation shape is irregular, suggesting that these bubbles could have less density and compactness than it should have to achieve stability.

This situation changes in figure 3.13, at a pressure of 1 GPa. As we can see, the aggregate has a more spherical and compact shape, looking more stable. Nevertheless, there are still particles that are not joined with the bubble formed. This is due to the periodic boundary conditions. This matches also with the figures seen before; bubbles formed at 1 GPa are stable enough, but if you increase its pressure, the stability and compactness can grow much higher.

However, this relation of spherical shape and stability should be confirmed by performing more simulations and comparing them.

The appearance of helium molecules at the opposite side of the box is caused by the boundary conditions set, which means that these isolated atoms are in fact part of the cluster.

Helium bubble radius

Using these results, we can analyze how the bubble radius evolves as a function of the pressure. For this purpose, we may look at the first peak of the RDF of the He-He interaction. The helium bubble radius was found by subtracting to the r value of the first RDF minimum (r_{max}) the r value of the first point before the first peak where the value of the RDF starts to grow (r_{min}).

$$r_{max}\text{-}r_{min} = r_{bubble} \quad \textbf{(19)}$$

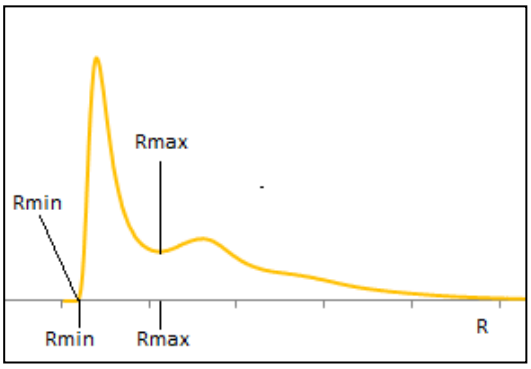

Figure 3.14: Criteria used for taking the values of r_{max} and r_{min}.

We summarize the results found in the following table:

Pressure (GPa)	Radius (A)
0.2	1.934
0.5	1.812
1	1.847
5	1.629
10	1.320

Table 3.1: Bubble radius as a function of the pressure.

At this point, it must be noticed that the results for pressure values under the 0.2

GPa pressure were discarded, as the bubble was not yet formed or was not consistent enough.

These results can also be represented in a plot, seeing how the radius evolves as a function of the pressure, and then try to figure it out the behavior of the bubbles if we increase the pressure. It should be considered that large pressures can change the bubble's radius evolution, especially if we are working with extreme values, so these results should be treated carefully and consider that we only know how the radius varies at this range of pressures.

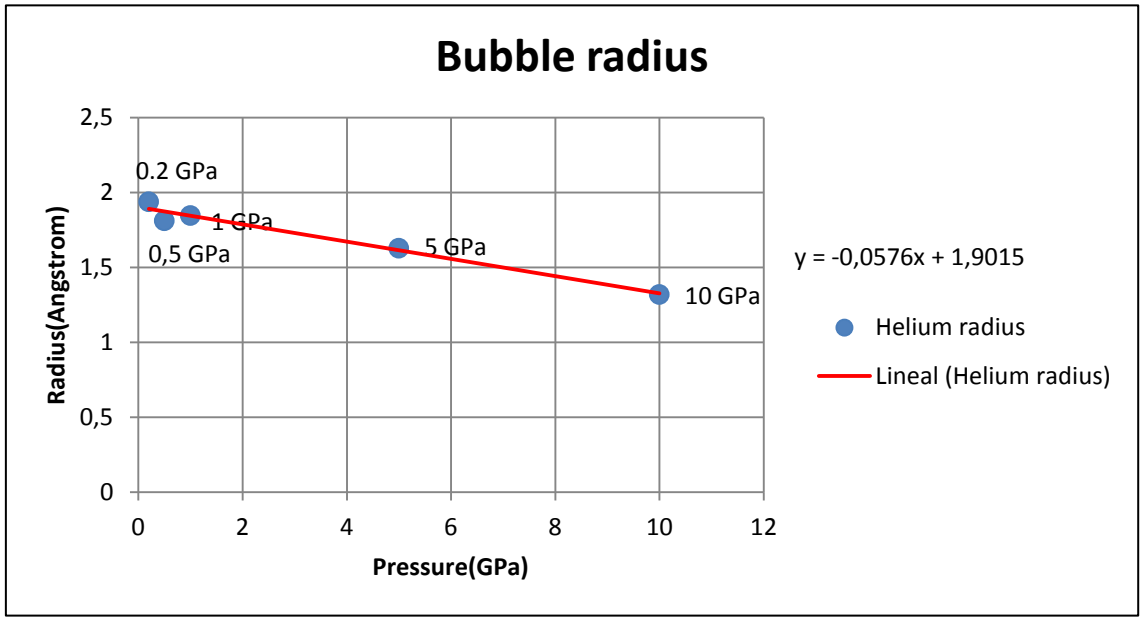

Figure 3.15: Radius evolution as a function of pressure at the range from 0.2 to 10 GPa.

As we can see in figure 3.15, the radius decreases when the pressure rises. This is totally logical and intuitive, as when we increase the pressure, the helium particles at the bubble are being more compressed, thus reducing its interatomic distances and also reducing the mobility of the helium particles.

This evolution has a clear linear tendency, being an easy task to extrapolate to higher values if the tendency remains unchanged, something we do not really know.

3.3. Dynamics

Mean squared displacement

It is also interesting to study bubble formation by looking at its dynamic properties. The Molecular dynamics algorithm gives us the possibility of computing two interesting parameters: the mean squared displacement and the spectra of the system.

As we explained before, MSD measures the deviation of the position of a

particle with respect to a defined reference position over time.

This parameter is especially important due to the fact that it can be used to compute the diffusion of the atoms in the system for every pressure. This can be achieved by means of looking at the MSD evolution for long simulation times, particularly at the last part of the graph. For large simulation times, the MSD evolution acquires a steady-state form, similar to a beeline. This means that for that part, the MSD evolves linearly, and we can compute its slope. The slope of this beeline is the limit of the MSD at $t \to \infty$, while equation (10) defines it as 6 times the diffusion of the atom that we are looking at. In short, if we have the slope of the steady-state of the MSD as a function of time, we are able to compute its diffusion coefficient D using the Einstein's equation.

For this reason, the MSD was computed for lithium and helium using the -1200 K potential at a temperature of 843 K and for pressures in the range from 0.1 to 10 GPa.

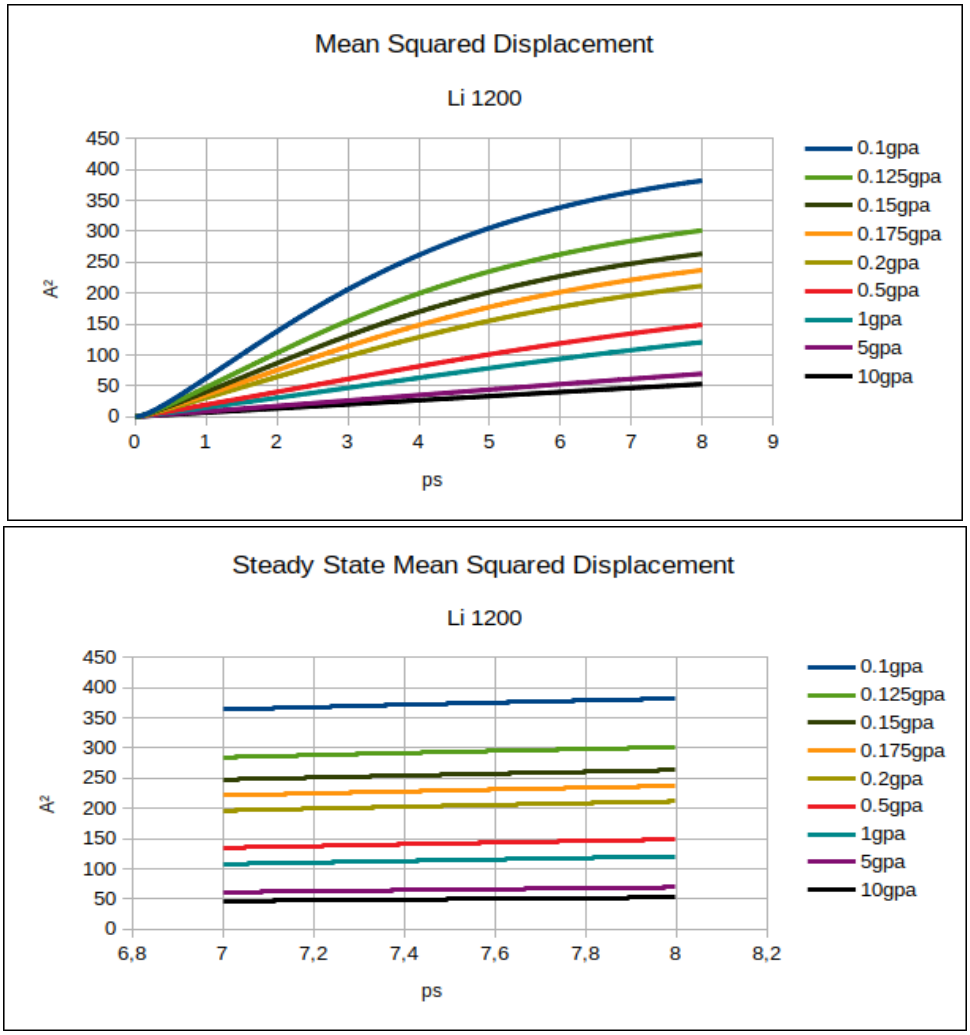

Figures 3.16 and 3.17: At the upper part, lithium MSD at a range of pressures from 0.1 GPa to 10 GPa and at the bottom part lithium MSD at the steady-state at a range of pressures from 0.1 GPa to 10 GPa.

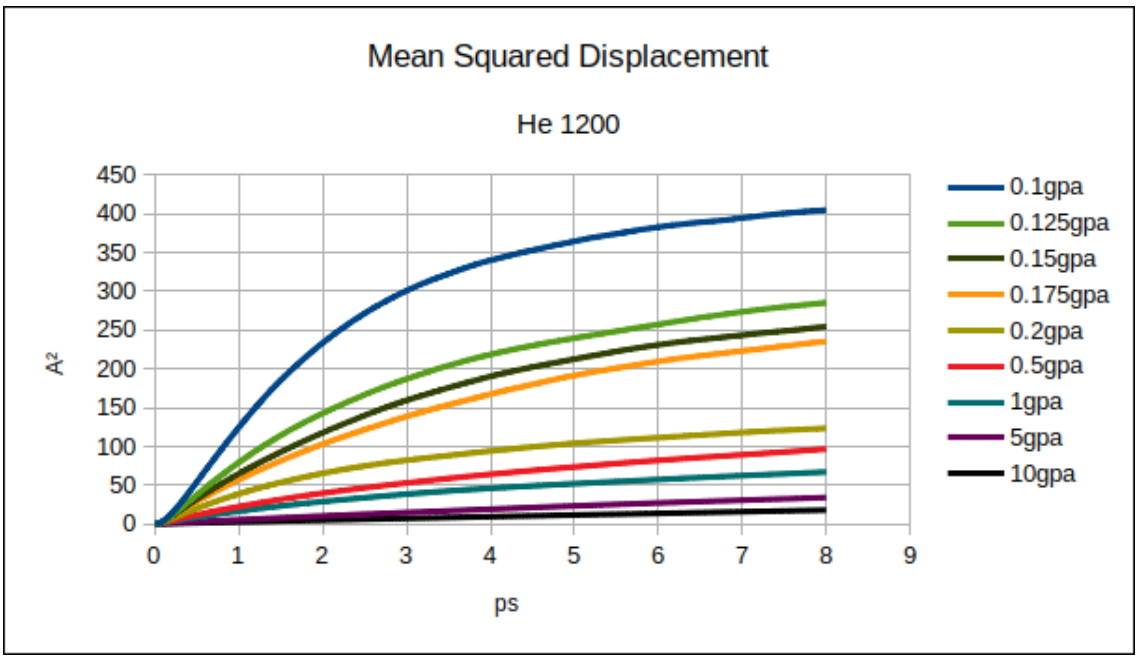

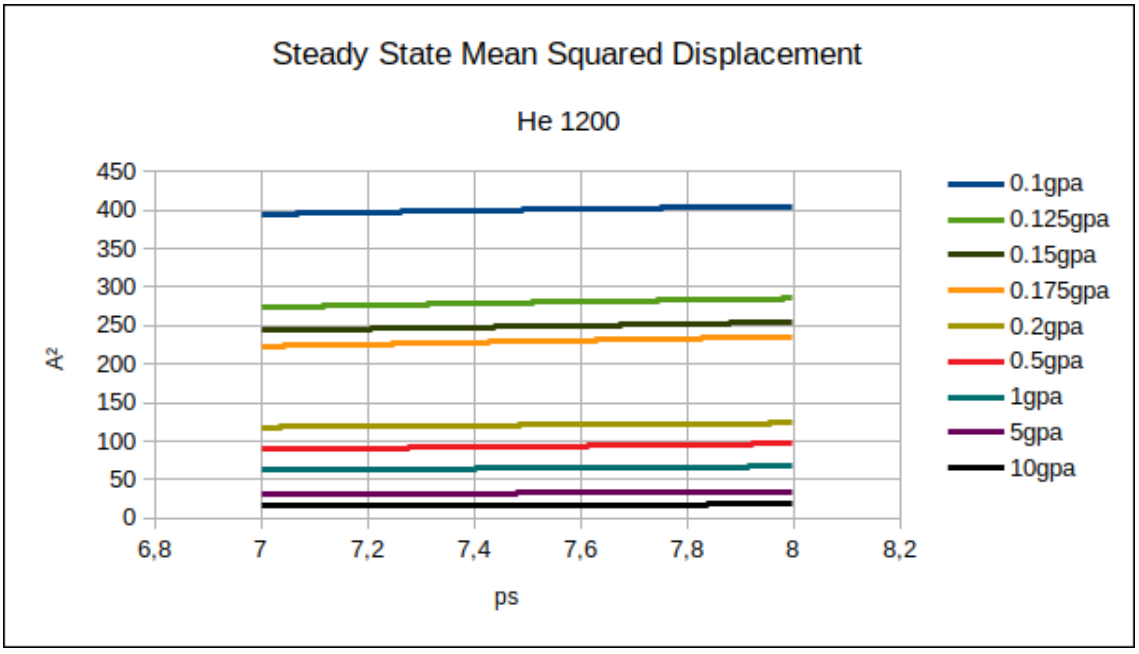

Figures 3.18 and 3.19: At the upper part, MSD of helium at a range of pressures from 0.1 GPa to 10 GPa and at the bottom part helium MSD at the steady-state at a range of pressures from 0.1 GPa to 10 GPa.

The slopes of all the steady-state beelines were extracted and the before mentioned method was applied, so slopes were divided by 6 and then the diffusion parameters for each pressure and each atom were obtained in A^2/ps.

The results must fulfill the constrain that D should decrease as we increase the pressure of the system because particle movement is limited due to the compression, so it is logical to find that this behavior takes place.

We can also find how this coefficient evolves in a graph with its evolution for both lithium and helium atoms at the range of pressures that goes from 0.1 GPa to 10 GPa.

Pressure (GPa)	D_{He} (A^2/ps)	D_{Li} (A^2/ps)
0.1	1.703	3.047
0.125	1.936	2.808
0.15	1.822	2.655
0.175	2.071	2.632
0.2	0.858	2.565
0.5	1.238	2.339
1	0.776	2.136
5	0.575	1.377
10	0.348	1.05

Table 3.2: Diffusion coefficient as a function of the pressure.

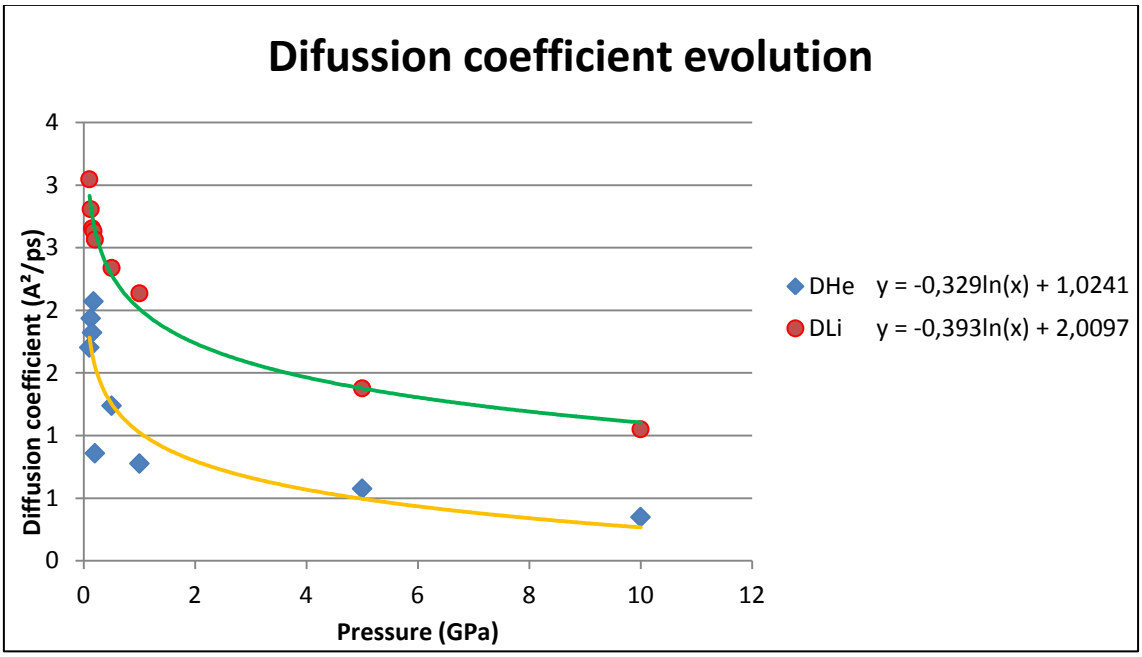

Figure 3.20: Evolution of the diffusion coefficient as a function of the pressure for a range from 0.1 to 10 GPa for He and Li atoms with their corresponding tendency lines equations**.**

As was expected, we see in figure 3.20, that the diffusion coefficient decreases as we increase the pressure, which it is a good signal. This means that the system behaves as it was expected. Also, we can see how the diffusion coefficient of lithium is larger than the diffusion coefficient of helium at the same pressure values.

By looking at his evolution as a function of the pressure, we see that there is a clear logarithmic tendency, from where we can extract the equations of the diffusion coefficient evolution for each atom. Another thing to notice is that, for both atoms, the values for the same pressure are different, while both tendency lines have almost the same form, which indicates that the evolution is similar even considering that they are different atoms.

We can compare these results with other reported in the literature to see if they fit.

For example, Canales et.al.[1] reported a diffusion coefficient of 2,47 A^2/ps at a temperature of 843 K at 1 GPa, while our result is 2,136 A^2/ps at this pressure, showing therefore a reasonable agreement.

Concerning helium, Nieto et.al. [9] obtained an experimental diffusion coefficient of 45 A^2/ps at 523 K and 1 GPa for a pumped system, i.e. in a regime of flow, which is much larger than our result of 0.77 A^2/ps and 843 K. This is due to different simulation conditions, as we are simulating a system at equilibrium, with no flow given by external forces.

Power spectra

As explained before, power spectra (PS) are obtained from the Fourier transform of the velocity autocorrelation function. It describes the main vibrational modes of the system. In other words, it indicates how the energy is distributed along different frequencies. This allows us to determine at which frequencies the atoms tend to vibrate.

Depending at which frequency the atom is vibrating, we can decide if that atom is doing a translational movement, it is bending, it is stretching or it is just rotating. In general, rotations and translations are related to low frequencies, and bending and stretching are related to high frequencies.

For this reason this property was computed for lithium and helium at different pressures, and then compared.

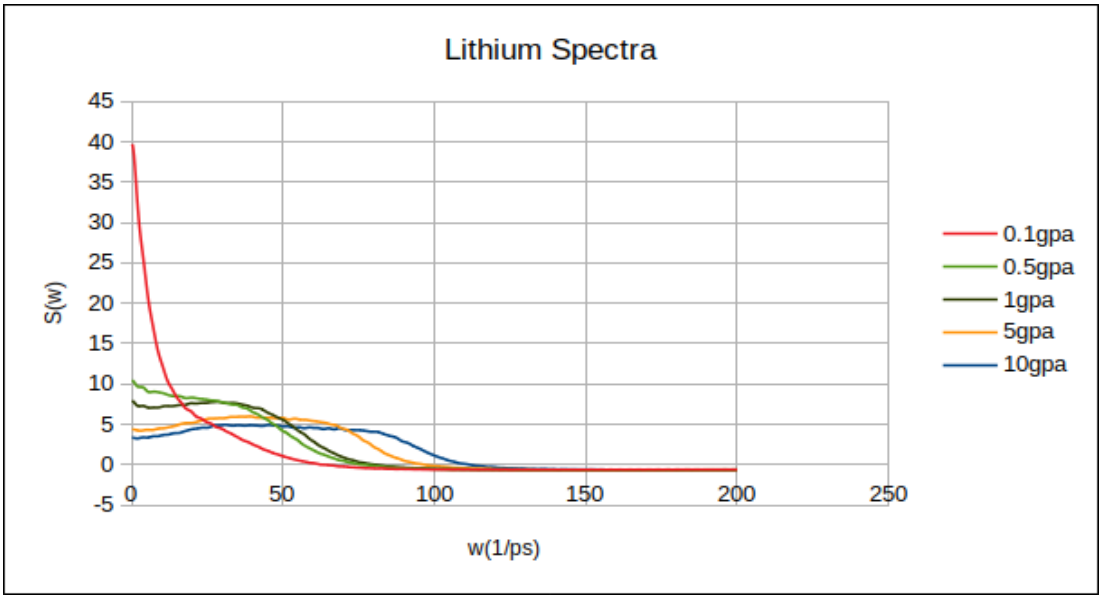

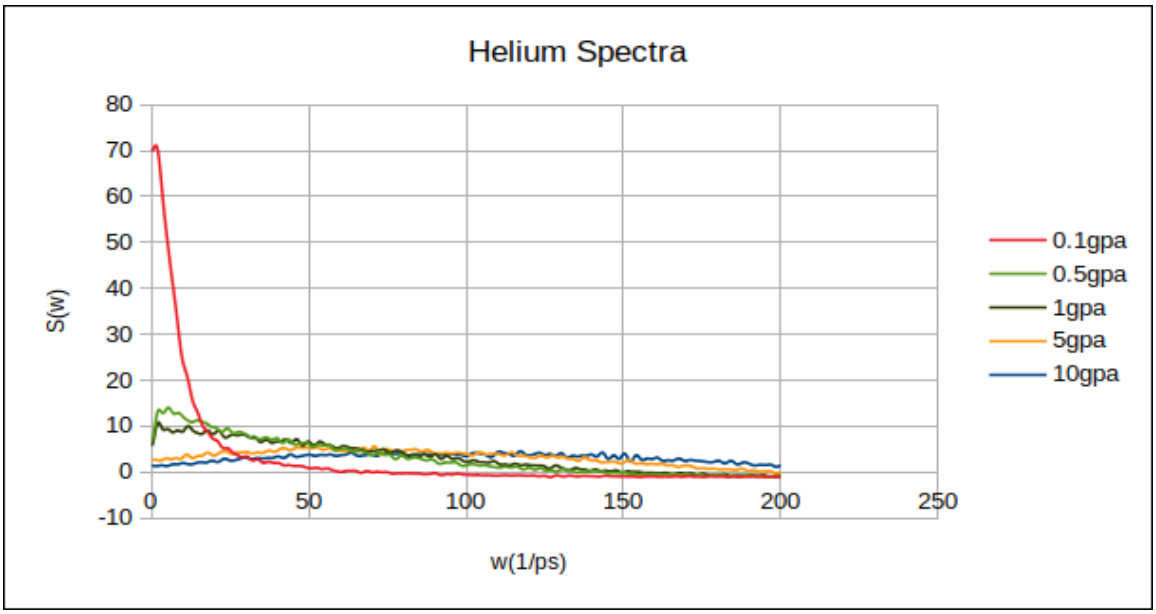

Figures 3.21 and 3.22: Respectively, lithium and helium power spectral densities for a range or pressures from 0.1 to 10 GPa.

As we can see in Fig. 3.21, the PS of lithium decreases as we increase the pressure. The peaks are also moved towards higher frequencies, while also getting wider. This means that when we increase the system's pressure, atoms tend to vibrate over a wider range of frequencies.

Similar thing happens with helium, as we can see in Fig. 3.22. At lower pressures the frequencies of vibration are very low and all the energy is concentrated in these frequencies. If we increase the pressure the peaks start decreasing and distributing along the entire frequency spectrum. At pressures of 5 GPa and 10 GPa, the power is spreaded in the whole frequency axis till 200 ps^{-1}, with a maximum approximately at 100 ps^{-1}. It is totally different at 0.1 GPa, where the vibration frequency is all concentrated around 2-3 ps^{-1}. Even considering that the energies and the shape of the spectra are different for both atoms, the behavior is the same: if we increase the pressure, the spectra gets wider and the maximum is displaced to larger frequencies.

As we explained in chapter II, vibrations around and above 500 ps^{-1} are related to bending and stretching modes, while vibrations under 100 ps^{-1} correspond to translational and rotational modes.

By looking at the plots, we can see that the PS value of both atoms does not increase in any frequency value around 500 ps^{-1}. This tendency continues for all the pressures, meaning that both atoms don't perform bending or stretching movements at any of the pressures simulated.

This fits well with the results of our simulation, due to the fact that we are considering single atoms, so they can only show rotational and translational

modes. This is due to the fact that single atoms don't have that many degrees of freedom.

Knowing this, the reason that makes the atoms to vibrate at higher frequencies if we increase the pressure of the system can be the fact that sets of atoms are being formed as we compress more and more the system, causing the atoms to vibrate in a wider range of frequencies.

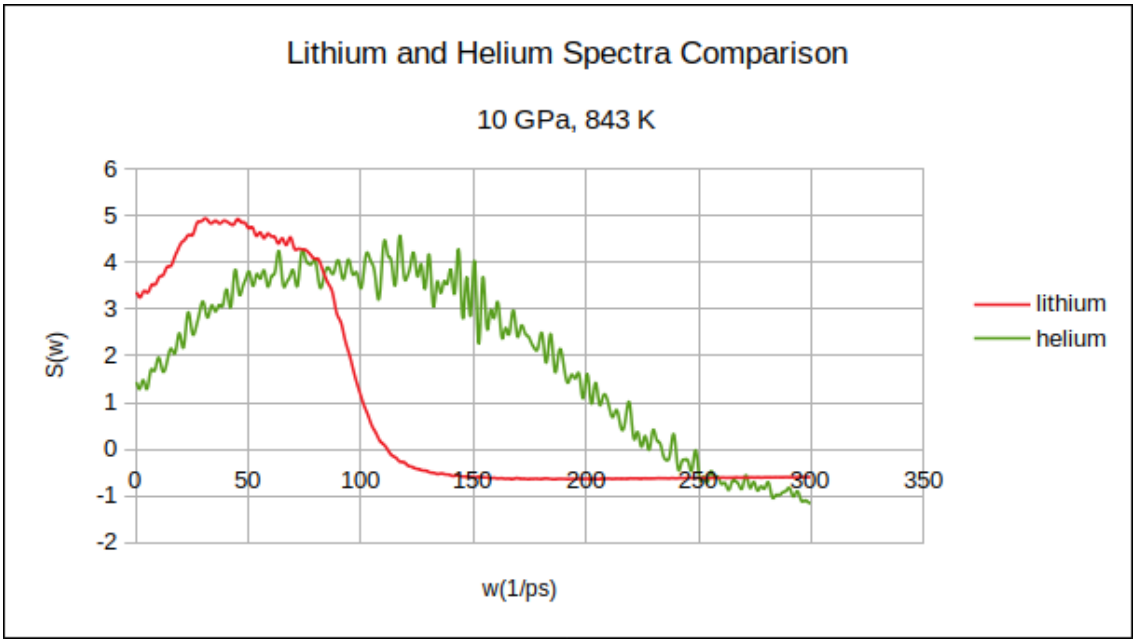

Figure 3.23: PSD of helium and lithium at 10 GPa.

Figure 3.23 compares us the PSD of helium and lithium at the same pressure of 10 GPa. This direct comparison shows that the helium peak is wider than the lithium peak, and is also more displaced to larger frequencies, which means that helium tends to vibrate at larger frequencies than lithium.

IV.CONCLUSIONS

Helium bubbles are an issue for the future usage of nuclear fusion reactors and it is a problem that must be studied. It is important to understand how these helium bubbles nucleate and how to avoid their presence in the reactors.

The MC and MD method can be used for solving problems related to nucleation bubbles, in particular the problem that we are facing in this work. Monte-Carlo is designed to describe systems at equilibrium, although it does not provide any information regarding the time evolution of the system. For that purpose MD is a better choice.

Even though the potential models used here seem to work relatively well, there are some issues that have not been solved, especially when we try to find its optimal parameters. This is partially

due to the lack of experimental data about helium while using the Lennard-Jones model. Without experimental data it is very hard to define a good simulation model. For our case, the potential parameter of the -1200 K model worked well and simulations demonstrated that it was a plausible choice. In fact, the model fits well with the radial distribution functions obtained by Canales et.al. [1] at 1 GPa.

We have seen how helium bubbles appear at some value between 0.175 and 0.2 GPa, which could be the signature of a phase transition from mixed to nucleated states, even though a passable level of stability would be reached at 0.5 GPa. However, even considering that there are bubbles formed at 0.5 GPa, they would not be able to reach a good stability and compactness level till the pressure value of 1 GPa. At this pressure, bubbles show more compactness and stability than the ones formed at 0.5 GPa.

Furthermore, we have shown that bubbles are more easily formed when the pressure is increased, and the more pressure we apply, the more stable it remains, being the bubbles more compacted and reducing its diameter.

This tendency is shown to depend linearly for high enough pressures, from 0.2 GPa, although we have only explored it up to 10 GPa. More studies are required to decide whether this linear behavior extends beyond that point. It is clear that bubbles cannot compress themselves forever. It should exist one value, from which the bubble radius will remain stationary, or it will collapse under immense pressures, but we do not know these limits.

The diffusion coefficient decays in a logarithmic way for both lithium and helium atoms when we increase their pressure, which is logical considering that the atoms are compressed and that constrains their movement.

On the other hand, the helium diffusion coefficients should be much larger than that of lithium, according to experimental reports, even considering that the 1 GPa value for helium seems to fit well with the experiments of Canales et.al. [1].

The Power Spectra are consistent in our simulations, showing that, due to the fact that they are single atoms, they vibrate at very low frequencies as they only have rotational and translational modes. This changes if we increase the pressure, increasing their frequency vibration and making the peaks wider, being able to oscillate at larger frequencies but never arriving to present stretching and/or bending modes.

It should be interesting to better understand bubble formation in this system, as this may be a key issue when building the ITER reactor. A continuation of this work could be to compute the surface tension of the formed bubbles and to analyze how the medium properties, pressure and temperature, can affect this result.

Furthermore, the breeding blanket of the ITER consists of Pb-Li materials, and thus it will be necessary to extend this study replacing Li with Pb. This means that experimental data about the LJ potential for Pb must be experimentally

collected prior to the simulation. All this can help us to understand the realistic system employed in the reactor, and to devise procedures designed to avoid undesired bubble formation. It is still a wide and an unexplored field to work with.

BIBLIOGRAPHY

[1] M. Canales, L. Gonzalez, and J. Àngel Padró. Computer simulation study of liquid lithium at 470 and 843 K. *Physical review. E, Statistical physics, plasmas, fluids, and related interdisciplinary topics*, 50:3656-3669, 12 1994.

[2] Laura Portos and Sandra Wells. Computational Simulation of Lithium - Helium Mixtures, *Universitat Politècnica de Catalunya, Department of physics*.

[3] M. Kordač, L. Košek; Helium bubble formation in Pb16Li within the breeding blanket. *Fusion Engineering and Design, November* 2017, 124:700-704.

[4] L. A. Sedano. Helium bubble cavitation phenomena in Pb-15.7Li and potential impact on tritium transport behaviour in HCLL breeding channels.

[5] Wirth, B.D.;Nordlund, K.;Whyte, D.G.;Xu, D. Fusion materials modeling: Challenges and opportunities. *MRS Bulletin*, March 2011, 36(3):216-222.

[6] P. Rosales-Pelaez, I. Sanchez-Burgos, C. Valeriani, C. Vega and E. Sanz. Seeding approach to nucleation in the NVT ensemble: The case of bubble cavitation in overstretched Lennard Jones fluids. *Physical review. E*, 101, 022611 (2020).

[7] Eduardo Oliva Gonzalo, Adriana Ortiz Gómez, Nuria Moral Fernández, Alejandro Carrasco Sánchez, José Manuel Perlado Martín, Raquel Suárez Hontoria, Manuel Cotelo Ferreiro, Curso básico de fusión nuclear, *Sociedad Nuclear Española*.

[8] Ronald A. Aziz, Frederick R.W. McCourt and Clement C.K. Wong. A new determination of the ground state interatomic potential for He_2. *Molecular Physics*, 61 (6):1487-1511, 1987.

[9] M. Nieto, D.N. Ruzic, J.P. Allain, M.D. Coventry and E.Vargas-Lopez. Helium retention and diffusivity in owning liquid lithium. *Journal of Nuclear Materials*, 313:646-650, March 2003.

[10] C. Di Paola, F. Sebastianelli, E. Bodo, F. A. Gianturco, and M. Yurtsever. Microsolvation of Li^+ in small He clusters. Li^+He_n species from classical and quantum calculations. *Journal of Chemical Theory and Computation*, 1 (5):1045-1054, 2005.

[11] D. Frenkel and B. Smit. Understanding molecular simulation. From algorithms to applications. *Academic Press*, 2002.

[12] A.S. Lemak and N.K. Balabaev. On the Berendsen thermostat. *Molecular Simulation*, 1994, Vol. 13, pp. 177-187.

[13] H. J. C. Berendsen, J. P. M. Postma, W. F. van Gunsteren, A. DiNola, and J. R. Haak. Molecular dynamics with coupling to an external bath. *J. Chem. Phys.* 81, 3684 (1984).

APPENDICES

Parameter	Value
a_0	$2.22125 \cdot 10^7$
a_1	41828.9
a_2	1.20145
a_3	1.84959
a_4	5.03762

Table A.1: Values of the constants for the equation (14).